CO-SIMULATION AND DYNAMIC ASSESSMENT OF THERMAL MANAGEMENT STRATEGIES ABOARD NAVAL SURFACE SHIPS

Submitted to:
The Office of Naval Research

Contract Number: N0014-08-1-0080

Submitted by:
T. Kiehne

December 31, 2013

Approved for Public Release – Distribution Unlimited

ELECTRIC SHIP RESEARCH
ESRDC
AND DEVELOPMENT CONSORTIUM

MISSION STATEMENT

The Electric Ship Research and Development Consortium brings together in a single entity the combined programs and resources of leading electric power research institutions to advance near- to mid-term electric ship concepts. The consortium is supported through a grant from the United States Office of Naval Research.

Florida State University

Massachusetts Institute of Technology

Mississippi State University

Naval Postgraduate School

Purdue University

University of South Carolina

United States Naval Academy

The University of Texas at Austin

2000 Levy Avenue, Suite 140 | Tallahassee, FL 32310 | www.esrdc.com

TABLE OF CONTENTS

LIST OF TABLES

LIST OF FIGURES

1 EXECUTIVE SUMMARY

The US Navy has committed to technology development for an all-electric ship (AES) that incorporates significant advances in power management, advanced sensors and weaponry, re-configurability, and survivability. Quantifying the close relationship between ship-board thermal, mechanical, and electrical sub-systems is of fundamental importance to understanding the nature of a large integrated system like the AES.

A critical impediment to efficient design has been that the existing tools make it difficult to couple the electrical and thermal behavior. In practice, however, they are closely coupled and critically interdependent. That impediment has been removed. This research shows that coupled solutions are possible in modern simulation systems.

Research efforts in support of this development have focused on physics-based, dynamic models of thermal components and subsystems that approximate, at the system-level, the notional architecture of an AES. This research has resulted in the development of a general purpose thermal management tool coded in C++ and known as the Dynamic Thermal Modeling and Simulation (DTMS) framework. The DTMS simulation environment provides the ability to model thermal systems and subsystems relevant to the AES. Using numerical approximations of complex physical behaviors, the scope of the DTMS framework has been expanded beyond elements of thermal-fluid behavior to capture the dynamic nature of far broader, more complex architectures containing interconnected thermal-mechanical-electrical components. The summary presented here describes the modeling approach used in DTMS and provides summary examples of its use in large, complex, system-level, dynamic simulations. These examples include:

- Thermal aspects of an integrated electric power system with component models for gas turbine engines, synchronous generators, motor converters, propulsion motors, and fixed-pitch propellers.
- Dynamic models for a marine vapor-compression chiller incorporating two-phase flow and heat transfer that is coupled to thermal loads representing shipboard compartment, thus allowing investigation of system response during full-load and part-load operation.
- Dynamic co-simulations that link a thermally dependent electrical power distribution network, and its consequent transient heat loads, with a thermal resistive heat flow network connecting these loads to the thermal management network at the system-level.
- Formulation of a state-of-the-art optimal controller, implemented in the marine chiller model, that accommodates dynamic heat loads while controlling the temperature of the chilled water and the refrigerant pressure and temperature in the evaporator.

Taken together, these examples demonstrate that DTMS is a sophisticated software platform capable of modeling and simulating complex physical systems, while simultaneously extending its ease of use for both the model developer and simulation user.

2 INTRODUCTION

The US Navy continues to support applied research on the design, development, and simulation of their future fleet of all-electric ships (AES). Central to the Navy's vision is the use of electricity as the primary energy transport means for the majority of ship systems. For example, ship propulsion has historically been handled by dedicated gas turbines connected directly to reduction gears, which drive a propeller. In the AES concept, prime movers are connected directly to generators, from which electrical power is sent to propulsors (via motor drives), and also to other ship systems.

The motivation behind this design approach is threefold. First, a future surface ship must be robust and reconfigurable; with an optimal power distribution grid, ship sectors damaged during combat can be isolated from the rest of the grid, thus minimizing damage and prolonging the ship's operability. Second, with a standard modular power grid, maintenance and cost of repair to ship power systems would be more efficient and cost-effective. Finally, the Navy expects to integrate various high-energy weapons and radar systems in future warships. An optimized power distribution grid would allow the ship to employ large pulses of energy required to implement these advanced systems. However, the introduction of advanced electronics and pulsed-energy systems on a surface ship is not without consequences. From a heat generation point of view, the AES will produce significant thermal side effects that have the potential to produce catastrophic failures at both the system and component level. Thermal management is considered an enabler for the technologies likely to appear on an AES.

Currently, the *Arleigh Burke* DDG-51 class destroyer employs five 200-ton marine chiller units to handle active cooling of ship systems and components. Every shipboard component, from the smallest processor chip to the largest gas turbine, contributes dynamically to this thermal management challenge due to the generation of "waste heat" that must be managed. It has been estimated [1] that, on average, approximately 681 tons of waste heat is rejected from an *Arleigh Burke* class warship. However, this average value does not capture the magnitude of peak waste heat during transient situations. On a highly dynamic, controls-oriented ship, such as the notional AES, steady-state values provide little utility from a reconfiguration or system failure perspective. When a fully capable AES is deployed, shipboard cooling requirements are predicted to have increased by as much as 700% [1]. However, this steady-state value does not include the integrated effects of dynamic power buildup and adaptive grid response following the introduction of high-energy weapons and sensors. It is the objective of the research reported in this paper to simulate shipboard thermal load management from a dynamic, controls-based, system-level perspective.

3 DYNAMIC THERMAL MODELING AND SIMULATION

At the outset of the AES program, no simulation tools were available to specifically address the following system-level issues:

- thermal aspects of high-energy power generation systems,
- robust electrical grids with dynamic re-configurability,

- high-density electrical storage capabilities,
- multi-megawatt pulse-load systems including advanced radar, sonar, and weaponry, and
- complex, adaptive thermal management systems.

Initial research efforts were focused on the use of two commercially available modeling tools to simulate thermal aspects of both current and near-term naval technologies. Steady-state representations were primarily accomplished using a general purpose software product created at the Delft University of Technology (Netherlands) called Cycle-Tempo [2]. This product was designed to address thermodynamic analysis and optimization for the production of electricity, heat, and refrigeration. Dynamic simulations were performed using a commercial power plant modeling tool called ProTRAX, which was developed over many years by the TRAX Corporation [3]. This product utilizes an adaptable FORTRAN programming base and a flow-effort approach to simulate commercial thermodynamic systems. The environment also features an integrated system of robust, tunable, feedback controls allowing for the generation of advanced and sophisticated training simulations. Notably, neither of these products is in any way oriented toward Navy-peculiar systems.

While these modeling tools proved immensely useful in early research efforts aimed at the simulation of thermal management systems for the AES, all commercial software packages ultimately present significant drawbacks that limit their suitability as a primary modeling tool for the US Navy. Due to relatively high investment costs, general lack of portability, and minimal customization options, research focus was ultimately directed away from utilization of commercial software and toward development of an in-house framework that is adaptable to complex model development. Specifically, the Dynamic Thermal Modeling and Simulation (DTMS) framework was developed to address system-level thermal management needs of the US Navy for next generation ship design.

The DTMS framework was created by UT graduate student Paullus [4] and improved upon by Pierce [5], who revamped the initial framework to create an updated version of DTMS with significant additional features. DTMS was developed from the ground up as a highly-customizable and universally-applicable analysis tool and has become the primary development system for thermal management work performed as part of the AES effort. DTMS grew into a sophisticated software platform capable of modeling and simulating complex physical systems while simultaneously extending ease of use for both the model developer and simulation user. It does not yet possess a front-end graphical user interface and documentation is limited to the thesis of various students, which are referenced here.

The DTMS framework was designed and implemented using the C++ programming language. This higher level language allows the user to take advantage of modern, object-oriented principles including encapsulation, inheritance, and polymorphism without sacrificing the performance required to accurately simulate highly complex physical systems. Six primary components are at the heart of DTMS, each of which fills a crucial role in development of a complete simulation. These components include *models*, *controls*, *fluids*, *solvers*, *output formats*, and a *simulation executive*. Each of these elements of the framework was designed to allow for user customization and permits the DTMS framework to be adapted and expanded to suit any

particular modeling need. The first four components, models thorough solvers, are briefly described below.

Models in the DTMS framework contain the algorithms and relationships required for simulating the behavior of a particular physical component. Each model exists independently from other components of the system, and thus, the physical behavior may be implemented using any method that best suits the application and the preferences of the model developer. By utilizing a common communication method between models and thus, eliminating reliance on boundary connections, models within DTMS are developed in isolation and in a generic manner that allows them to be used to create indefinitely large system simulations that may be reused by others to address additional applications or system configurations. This modular design approach allows complex components to be independently designed, implemented, and tested before insertion into a larger simulation. For example, a gas turbine engine may be constructed within DTMS from sub-models for a compressor, combustor, turbine, and rotating shafts such that, when tested and validated, these may be combined to form a complete, self-contained engine model that can then be used in a more complex system representation.

While the modeling approach in the DTMS framework promotes the use of self-contained, independent sub-models, the DTMS controls system is composed of a series of building blocks that allow customized controller networks to be created in a manner most applicable to the development task at hand. These control elements are designed to allow a simulated system to maintain stability and respond to dynamic events during the execution of a simulation. A block diagram approach consisting of four basic elements was used to construct the architecture of a control system. These elements are a source, a summer, a transfer function, and a sink. These building blocks may be arranged by the developer or simulation user to create both open and closed feedback loops possessing a wide variety of characteristics. All simulations using DTMS thus far have utilized a manually-tunable, PID controller constructed from these components. While the controls system is currently the least advanced feature of DTMS, recent work focused on implementing elements of modern control theory in this framework. In particular, the work of Salhotra [6] that is reported here has added considerable flexibility and reliability to the controls modeling in DTMS.

In order for fluid flow networks to remain useful for a variety of engineering applications, the fluid flow models within the DTMS framework were designed to easily adapt to custom, user-defined fluid property routines that are defined within the framework using customized DTMS fluids. The generic nature of these property calculators allow the fluid flow components in DTMS to be utilized with any thermodynamic fluid applicable to a given application. These customized fluid routines utilize a variety of assumptions about the properties of a specific fluid. For example, if a simulation system utilizes low Mach number gaseous flow, then property calculators based on ideal gas assumptions are used in order to speed up the simulation calculations. If fluid flow with a phase change is involved, the fluid flow models utilize a fluid property calculator based on empirical data to compute accurate representations of the fluid state. DTMS also provides an interface to the National Institute of Standards and Technology Reference Fluid Thermodynamic and Transport Properties (REFPROP) [7] database to permit use of detailed property equations for numerous multi-phase fluids. The simulation user is free to

select fluid property calculation routines which provide the best combination of speed and accuracy for a given application.

While models in the DTMS framework were designed to operate in isolation, physical conservation laws are typically applied across an entire system during the course of a simulation. Thus, numerical solvers were implemented in the DTMS framework to calculate dependent variables that particular models are unable to, or choose not to, handle internally. Depending on the type of modeling method utilized in a simulation, DTMS employs a variety of standard solvers that implement solution routines having various benefits as well as limitations. Linear system solvers may be used for initial simulations where accuracy may be sacrificed for speed, while nonlinear solvers may be utilized when more accuracy is required. Similar to other aspects of the framework, the solvers were designed in a modular fashion that allows the simulation user to select the modeling technique or solution method most appropriate for a particular application, or to formulate any alternative solution technique that might be advantageous.

Using customization features provided by each of the above components, the DTMS framework allows users and developers to construct and analyze complex, useful, and meaningful simulations of real-world systems with dynamic, transient effects spanning across thermal, mechanical, and electrical boundaries. The modular, object-oriented nature of the software design allows the framework to adapt and expand as new capabilities are introduced. After an introduction to the modeling architecture, summary examples of the use of the DTMS framework are presented below.

4 RESISTIVE NETWORK MODELING

The DTMS framework is capable of incorporating and managing any number of modeling strategies. Thus, initial efforts were focused on a common modeling strategy that allows for consistent model development while providing a structure for developers to build upon using other modeling strategies as desired. Based on lessons learned in using commercial software referenced earlier, a Resistive Network approach was chosen as the primary modeling strategy for use in the DTMS framework. The Resistive Network modeling approach is applicable to numerous energy domains, has a component-independent modeling philosophy, allows multiple layers of detail, and results in relatively straightforward solution methodologies. This modeling approach requires that the constituent equations of a system be organized such that they represent resistive loads on a network. Although Resistive Network modeling can be applied to systems of many different energy domains (electrical, thermal, fluid, mechanical, rotational, etc.), the method is most commonly demonstrated by analogy with an electric circuit consisting of a series of resistors connected together in a network with one or more voltage or current sources, as shown in Figure 1.

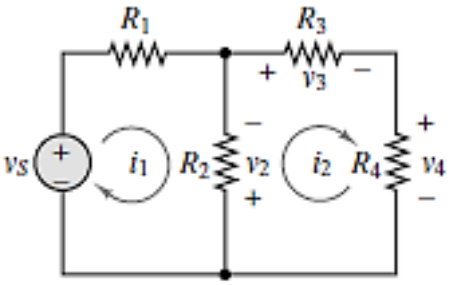

Figure 1: Example of an electrical Resistive Network

4.1 Flow Models

In a Resistive Network, flow-based models are used to represent physical components using a quasi-steady flow driven by a difference in effort between inlets and outlets. Thus, at each point in time, the amount of flow entering a model through the inlets must be identical to the amount of flow exiting the model through the outlets. While the value of the flow rate may vary between successive time steps, there can be no storage of flow within a flow-based model. Components represented by this type of model conform to the following general flow-model equation:

$$f = \phi\left(e_{i,1}, e_{i,2}, ..., e_{o,1}, e_{o,2}, ...\right). \qquad (1)$$

The generic flow function (ϕ) is composed of each inlet effort $\left(e_{i,1}, e_{i,2}, ...\right)$ and outlet effort $\left(e_{o,1}, e_{o,2}, ...\right)$ associated with the model, and these produce the component flow for the entire model (*f*). Referring to the electrical circuit example in the figure, the constituent equation for a linear electrical resistor is:

$$i = \Delta V/R \qquad (2)$$

where *i* is the current through the resistor, ΔV is the voltage drop across the resistor, and *R* is the linear resistance. Comparing this with the general flow-model equation, *i* represents the flow *f*, ΔV the difference between the inlet effort $e_{i,1}$ and outlet effort $e_{o,1}$, and $\Delta V/R$ the generic function ϕ. Based on this linear resistance equation, the electrical resistor conforms to the general flow-model equation, and therefore is considered a flow-based equation.

4.2 Effort Models

Since flow-based models require their inlet and outlet efforts to be specified by bounding models in order for the flow to be calculated, two flow models cannot be directly connected together since neither would be able to provide the effort for the other. Effort-based models provide the data required to complete the model connections of a simulated system. Most often, effort-based models are used solely for this purpose and do not represent any physical component, i.e., they exist merely as a modeling construct necessary for resolving the system. However, while commonly used for connecting flow models, effort-based models can also represent certain physical models such as mixing chambers, combustion chambers, or other flow junctions. Regardless, the vast majority of physical components are represented with flow-based models.

Effort-based models in a Resistive Network represent components that have a single effort throughout the model and maintain conservation of flow across inlets and outlets. Primarily, these models are governed by a general effort-model equation based on flow conservation:

$$\sum_{j=1}^{m} f_{i,j} - \sum_{k=1}^{n} f_{o,k} = 0 \qquad (3)$$

where $f_{i,j}$ is the j^{th} inlet flow and $f_{o,k}$ is the k^{th} outlet flow. Similar to flow-based components, this equation requires quasi-steady flow throughout the effort-based model, which in turn requires that quasi-steady flow be maintained throughout the entire system. In many systems, particularly thermal-fluid systems, this limitation is inconsequential to achieving the required simulation result. However, it can become overly limiting in other systems, particularly electrical systems.

4.3 Inertial Models

Unlike resistive elements, which rely on the relationship between flow and an effort for a particular model, inertial elements are largely concerned with the concept of the motion of a system, which is often referred to using the generic term "momentum". The concept of momentum is widely understood in mechanical systems. It is represented by linear momentum in translational systems and angular momentum in rotational systems. Other types of systems typically represent the momentum based on its relation to a flow variable. Electrical systems refer to momentum as the infrequently-used magnetic flux linkage, while thermal and chemical systems have no unique term to represent this quantity.

Generalized momentum is most frequently defined by its relationship to the efforts of a system; specifically, an effort is equivalent to the time-derivative of the momentum:

$$\dot{p} = e \qquad (4)$$

where p is used to represent the momentum and e again represents an effort. Whereas resistance elements are represented by constitutive relationships relating the flow to an effort, inertial elements are represented by constitutive relationships relating the flow to the momentum:

$$f = \phi_I(p). \qquad (5)$$

However, this expression is not compatible with the techniques utilized in the Resistive Network modeling strategy as it does not directly relate a flow to an effort. Fortunately, this constitutive relationship for an inertial model may be represented in terms of a functional relationship between the flow and the time-integral of the effort:

$$f = \phi_I\left(\int e \cdot dt\right). \qquad (6)$$

Inertial models may be developed within the Resistive Network modeling strategy so long as the time-integral of the effort can be calculated. While this is virtually impossible to accomplish analytically without explicit knowledge of every flow equation in the system, the time-integral of the effort may be calculated numerically using an approach called the Closed Newton-Cotes formulation [8]:

$$p_{4n+1} = p_{4n} + \frac{h}{2}\left(e_{4n} + e_{4n+1}\right) \tag{7}$$

$$p_{4n+2} = p_{4n} + \frac{h}{3}\left(e_{4n} + 4 \cdot e_{4n+1} + e_{4n+2}\right) \tag{8}$$

$$p_{4n+3} = p_{4n} + \frac{3h}{8}\left(e_{4n} + 3 \cdot e_{4n+1} + 3 \cdot e_{4n+2} + e_{4n+3}\right) \tag{9}$$

$$p_{4n+4} = p_{4n} + \frac{2h}{45}(7 \cdot e_{4n} + 32 \cdot e_{4n+1} + 12 \cdot e_{4n+2} + 32 \cdot e_{4n+3} + 7 \cdot e_{4n+4}) \tag{10}$$

where p represents the momentum, e the effort, h the simulation time step, and n is an integer that identifies data at a particular time. These equations form a series of approximations, with increasing order of accuracy, that are employed based on the amount of information available during a time step. The accuracy of these may be increased by decreasing the time step in the overall system simulation.

4.4 Capacitive Models

While the property "inertia" is not commonly expressed in the fundamental equations of various types of physical systems, "capacitance" is widely used throughout these systems. Capacitance may represent springs in a mechanical system, actual capacitors in an electrical system, and storage tanks in a fluid system. Capacitive elements are characterized by the storage of potential energy through "displacement" of a flow.

Similar to the relationship between generalized momentum and an effort used to represent inertial behavior, capacitive behavior is characterized using the following relationship between flow and displacement:

$$\dot{q} = f \tag{11}$$

where q represents a generalized displacement and f represents the generalized flow. The constitutive relationship between displacement and effort is defined using a generic capacitance function, ϕ_C, where

$$q = \phi_C(e). \tag{12}$$

Like its inertial element counterpart, this constitutive equation is not initially compatible with resistive networks. However, it can be transformed into a flow-effort equation by combining the previous two relationships into a single equation that relates the generalized flow to the effort:

$$f = \frac{d}{dt}(\phi_C(e)). \tag{13}$$

This result allows capacitive elements to be simulated using the Resistive Network modeling strategy so long as the time-based derivative can be simulated within the capacitive model. Like integral approximations used in the inertial models, it would be difficult to directly differentiate this capacitive function without intimate knowledge of all flow equations in the network. However, numerical approximations of this derivative can be implemented that allow the capacitive behavior to be simulated without requiring an exact solution to this differential equation.

While various techniques exist for generating a numerical approximation of a derivative, the nature of the DTMS framework prevents the use of data from future time steps. Thus, backward difference schemes [9] have been employed for capacitance models in the DTMS framework. For the first three simulation time steps, flow through the capacitive element is calculated using first-, second-, and third-order backward differencing schemes, respectively. These are presented as:

$$f_1 = \frac{q_1 - q_0}{h} \tag{14}$$

$$f_2 = \frac{3 \cdot q_2 - 4 \cdot q_1 + q_0}{2h} \tag{15}$$

$$f_3 = \frac{11 \cdot q_3 - 18 \cdot q_2 + 9 \cdot q_1 - 2 \cdot q_0}{6h} \tag{16}$$

$$f_n = \frac{25 \cdot q_n - 48 \cdot q_{n-1} + 36 \cdot q_{n-2} - 16 \cdot q_{n-3} + 3 \cdot q_{n-4}}{12h} \tag{17}$$

where f represents the flow, q the displacement, h the simulation time step, and n is an integer greater than 3 that identifies data at a particular point in time. In each formula, the error is a function of the time step; thus, the error is on the order of h, h^2, h^3, and h^4 for the first-, second-, third-, and fourth-order equations respectively. As with inertial components, the accuracy of the capacitive components may be increased by decreasing the time step in the overall system simulation.

4.5 Solution Methods

The models that compose the Resistive Network modeling strategy were designed specifically to construct the overall flow network in a predictable and repeatable manner. This consistent nature allows a system to be resolved using generic methods that need not be specialized for each individual simulation. Within the system being modeled, the only dependent variables are the effort values contained in effort models. By enforcing conservation of flow within each effort model, the time-dependent solution for these values may be calculated using common matrix methods.

In a system consisting strictly of linear flow models, or linear approximations of nonlinear flow models, a solution for the efforts in the system is calculated using:

$$\overline{C}_D \bar{e}_D + \bar{f} + \overline{H} + \overline{C}_I \bar{e}_I = 0 \tag{18}$$

where C represents the vector of time-dependent flow coefficients, e is the effort vector, f is the flow vector, and H is the vector of time-dependent effort source terms. The subscripts D and I indicate dependent and independent values. This system of equations is solved using matrix methods to yield the dependent effort vector.

For systems that consist primarily of nonlinear flow models, the system efforts cannot be resolved directly and must be calculated iteratively. Within DTMS, the Newton-Raphson method [10] is used as the nonlinear iteration method of choice due to the accuracy and rapidity with which it converges to a solution. Using a Taylor series expansion of flow conservation for each

dependent effort model, the Newton-Raphson solver iterates on the following system of equations until conservation of flow is achieved.

$$\bar{e} = \bar{e}_o - \bar{\bar{J}}^{-1} \bar{f}(\bar{e}_o). \tag{19}$$

Here e is the potential vector at each node, e_o is a reference effort vector, f is the flow vector, and J is the Jacobian matrix composed of partial derivatives of the flows. While the Newton-Raphson method can suffer from instability when an intermediate iteration begins far from the solution, this behavior has been well studied in the literature, and numerous compensation routines are available to overcome this limitation. One such routine, referred to as the globally convergent Newton-Raphson method has been implemented in the DTMS framework.

5 SIMULATION EXAMPLES

For several years at the University of Texas, the DTMS framework has been in exclusive use at the University of Texas on behalf of the Navy's system-level, thermal management program. It has been employed in a variety of dynamic simulations including aspects of a shipboard integrated electric propulsion system [11], a marine chiller system involving large-scale, thermal load management [12], and thermo-electric co-simulation of shipboard power conversion systems [13]. Finally, work has recently been completed on implementation of a modern control system within the framework [6].

Space limitations permit only a selected summary of results coming from these studies; details are contained in the source documents referenced. The intent in what follows is to summarize the work that has been done and also to demonstrate the flexibility, adaptability, utility and general purpose nature of the DTMS framework.

5.1 Integrated Electric Propulsion System

Holsonback [11] developed and validated a dynamic, thermal-mechanical-electrical model of the integrated propulsion system (IPS) on a notional AES in ProTRAX [3]. This IPS model was used to simulate ship maneuvers and resultant mechanical-electrical-thermal effects. The simulation included representations of the main and auxiliary gas turbine engines, synchronous generators, motor converters, propulsion motors, fixed-pitch propellers, and a ship hull. These component models were integrated into a system-level simulation and validated against dynamic results for acceleration from full-stop to cruise, and for a warship maneuver called a "crash-back", an emergency reversal of direction. These simulations include megawatt-sized heat loads in the electric generators and propulsion motors. Pierce [4] recreated and validated this model in DTMS. The variable flow in this simulation is represented in Figure 2.

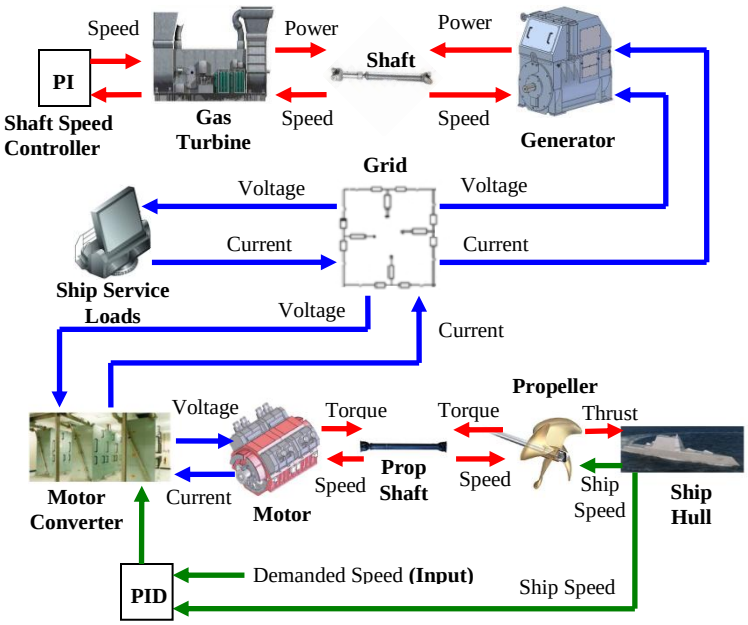

Figure 2: Variable flow in dynamic IPS model at runtime.

Figure 3 depicts the dynamic evolution of motor speed and power during a crash-back event. Ship speed is steady at 29.4 knots ahead with a single motor mechanical power of 17.2 MW (68.6 MW total) at 119.4 rpm. The demand then quickly transitions to -100% during which the motor mechanical power ramps down at a rate of approximately 2 MW/s. The motors begin regenerating at 1 MWe within 20 seconds of the initiation of crash-back. During regeneration, which lasts for about 40 seconds, both the motor and ship speed fall modestly. When the motor speed becomes negative, the motor power returns to positive, signaling that the motors are now operating in the astern direction. The motor and ship speeds then fall relatively quickly, until about 75 seconds into the crash-back at which time the motors exhibit a hesitation in their speed due to interaction of the propeller and ship, and the torque limitation of the propulsion motors. The ship speed passes through zero at about 95 seconds into the crash-back; this is denoted as "time-to-stop." After this point, the motor power, motor speed, and ship speed increase quickly to their steady state values. The ship ends the crash-back at -26.8 knots with a single motor mechanical power of 17.5 MW (69.9 MW total) at -121.7 rpm. The power difference between the ahead and astern condition is caused by the characteristics of the propeller and the assumed Taylor wake fraction.

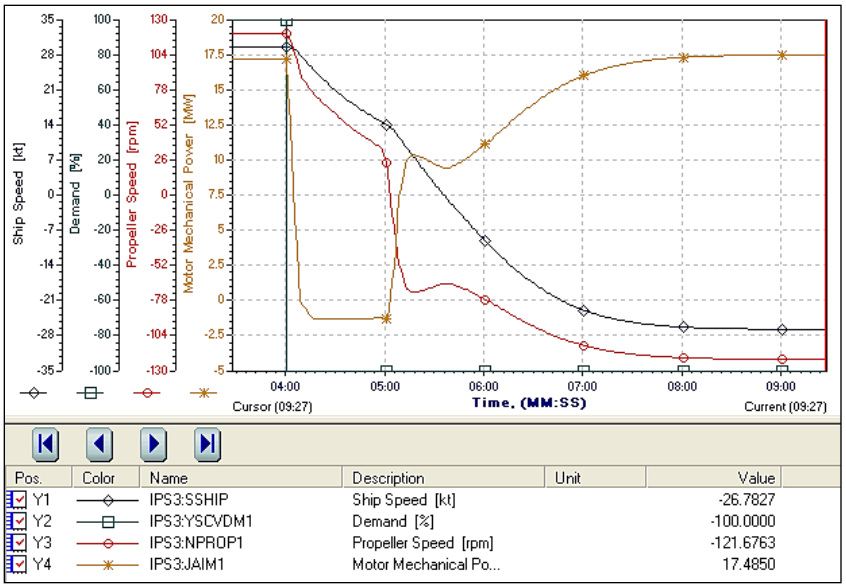

Figure 3: IPS ship and motor speed and motor power during crash-back.

Generators, motors, and converters are all significant sources of waste heat in the IPS. As simulated in DTMS, Figure 4 illustrates the evolution of these heat loads during a crash-back. At the beginning of the maneuver, each of the twin main and auxiliary gas turbines (MGT and AGT) produces approximately 726 kW and 200 kW of waste heat (1.85 MW total) both before and after the crash-back. Each motor-converter pair produces 1.38 MW of waste heat (5.5 MW total). Therefore, a total of 7.35 MW of waste heat, not including gas turbine exhaust energy, is created by these components. The transient depicted during the crash-back reflects motor regeneration and transitory heat output from each of the drive train components that occurs during transition from regeneration to motoring astern. Hesitation of the propulsion motors during astern motoring is clearly reflected in the waste heat of the motor-converter pair. Simulation results indicate that the propulsion motors and associated converters produce the largest thermal loads in the propulsion system.

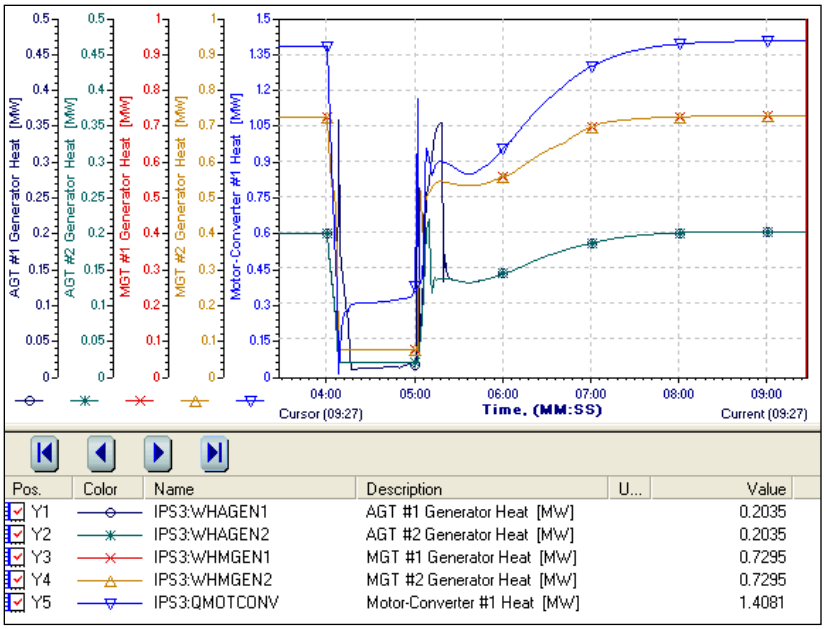

Figure 4: Generator and motor-converter waste heat during crash-back.

Direct comparison can be made between the crash-back results presented above and simulations of a notional destroyer-class, all-electric ship presented in Andrus, et al. [14]. The integrated power system components presented therein are very similar to those utilized in this analysis. In Figure 5, the background results are the same as those shown in Figure 3. The inset from Andrus, et al. is for a ship crash-back from 30 knots, with approximately 30 MW on each shaft at 110.3 rpm, to -5 knots, with approximately 30 MW per shaft at -75 rpm, over a period of about 80 seconds. Their simulation also incorporates a 15% motor power ramp rate limit per second and 4 MWe regeneration limit. Scaling the inset to match the scale of the background plot gives the image shown. Clearly, the same characteristic motor speed versus time shape is exhibited by each of these IPS system models. However, because of the higher rated torque, slower initial rotational speed, and higher power ramp rate limit, the crash-back response from Andrus, et al. is clearly faster than that obtained in this analysis; they reported a time to stop of 63 seconds versus the approximately 95 seconds found here.

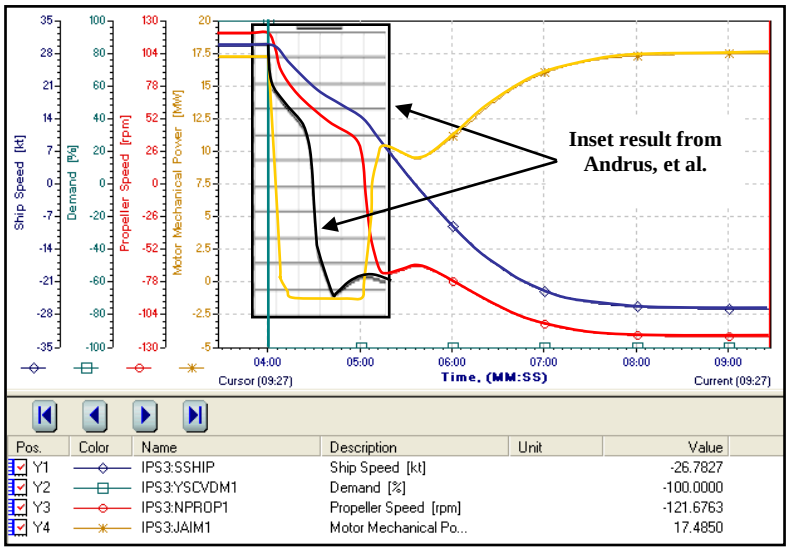

Figure 5: Comparison of crash-back results to those of Andrus et al. [14].

5.2 Thermal Load Management of a Dynamic Chiller

Hewlett [12] augmented DTMS to model two-phase flow and heat transfer for simulation of a shipboard vapor-compression chiller and its attendant loads. The controls methodology implemented in the heat exchanger models monitored their relevant states and refrigerant liquid levels. Models for these heat exchangers along with those for a centrifugal compressor and thermostatic expansion valve were used to simulate a 200-ton marine chiller using baseline parameters for the US Navy's current destroyer. This chiller was then connected with thermal loads of varying magnitude to demonstrate controller response during full-load and part-load operation. The largest simulation consisted of 22 thermal loads ranging from 8 to 256 kW with chilled water supplied by two chiller units. The system configuration is shown in Figure 6. Each thermal compartment is represented by a specified passive heat input and employs a valve controller to monitor return chilled water enthalpy. Since the total heat load is 1324 kW split among 22 compartments, two 200-ton chillers are necessary for load management. Note that the York #1 chiller is closest to the largest thermal loads in the simulation, 3W and 4W. These loads are due to ship-based radar and defense electronics packages.

Figure 7 shows the temperature response of each thermal load as simulated in DTMS. As expected, both the load magnitude and its proximity to a chiller impact thermal response. Thus load 9W, the largest load located furthest from a chiller attains the peak temperature in this system. Due to the 80 meters that the chilled water must travel, load 9W is also the last to reach the set point, at approximately 600 seconds.

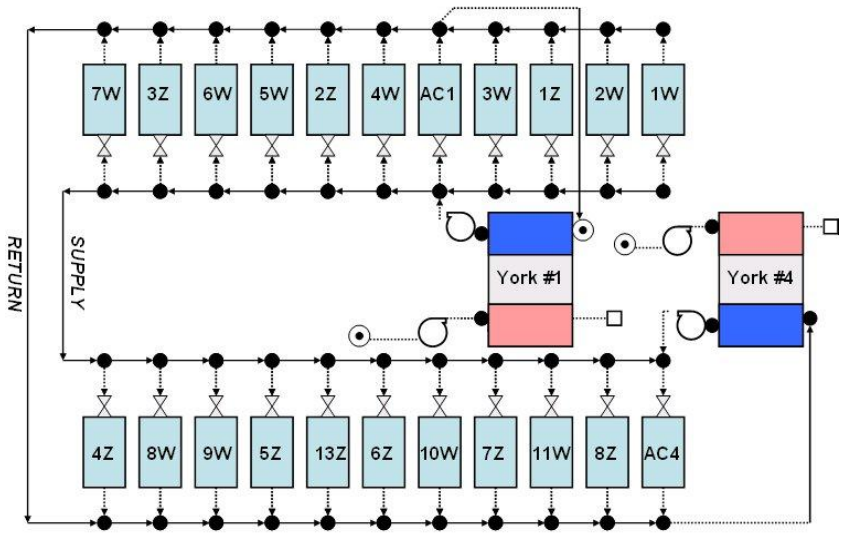

Figure 6: DDG-51 starboard chilled water loop configuration.

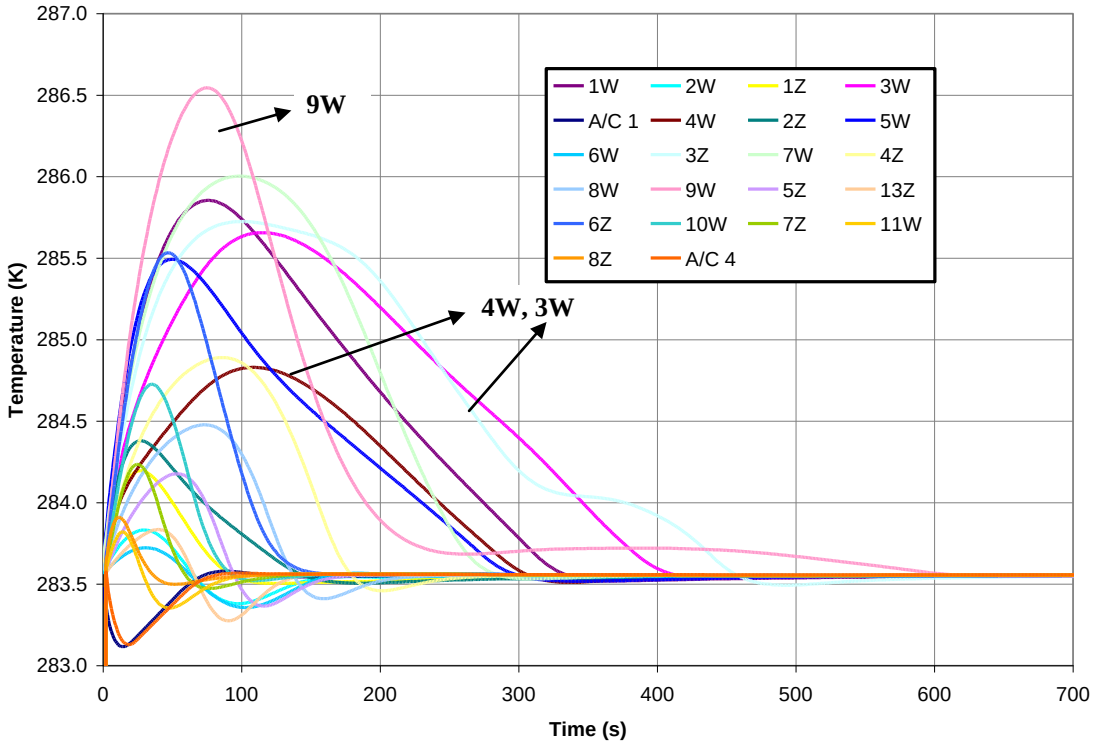

Figure 7: Starboard loop at start-up: load temperatures vs. time.

The above simulation indicates the potential for use of DTMS as a tool to investigate technology alternatives for shipboard implementation. In fact, several non-traditional shipboard cooling concepts have already been implemented in DTMS and compared against current chilling systems. One example is presented below.

Any HVAC system that provides heating or cooling without variably adjusting the flow of air is characterized as constant-air-volume (CAV). HVAC on current US Navy surface ships employs CAV ventilation [15]. With many years of application and refinement, CAV HVAC does have its advantages. The costs of CAV-capable equipment (fans, ductwork, controls, etc.) are markedly less than alternatives. From a controls standpoint, the adjustment of chilled media temperature is relatively straightforward, and constant-speed, on/off fan control is simpler than variable-speed control. In fact, for a small to moderately sized facility, CAV is undoubtedly the most advantageous option. However, in larger structures such as a naval surface ship, CAV has a number of disadvantages. For example, current HVAC strategy on the DDG class destroyer applies a worst-case cooling strategy in that marine chillers designed into warships have the capability to manage every time-dependent load at its peak value. Obviously, a worst-case condition is rare. However, CAV mandates constant air flow without regard to part-load behavior. As a result, shipboard airflow is often markedly higher than necessary. This not only represents many kilowatts of wasted energy and cooling capacity, but it also prevents shipboard HVAC from dynamically handling time-dependent loads and other events via reconfiguration.

Consider a thermal compartment similar to the thermal loads represented in Figure 6. However, to support an HVAC simulation, air flow is now modeled in a separate but related flow network consisting of a fan, air-handling unit (AHU), and cooling-coil heat exchanger (CCHX). Ambient air is circulated using a constant-speed fan driving air through a fan coil unit (FCU), represented by a series of ducts and the CCHX. The chilled freshwater supply absorbs thermal energy from the compartment via the circulating air, and the warmer return is directed back to the chiller.

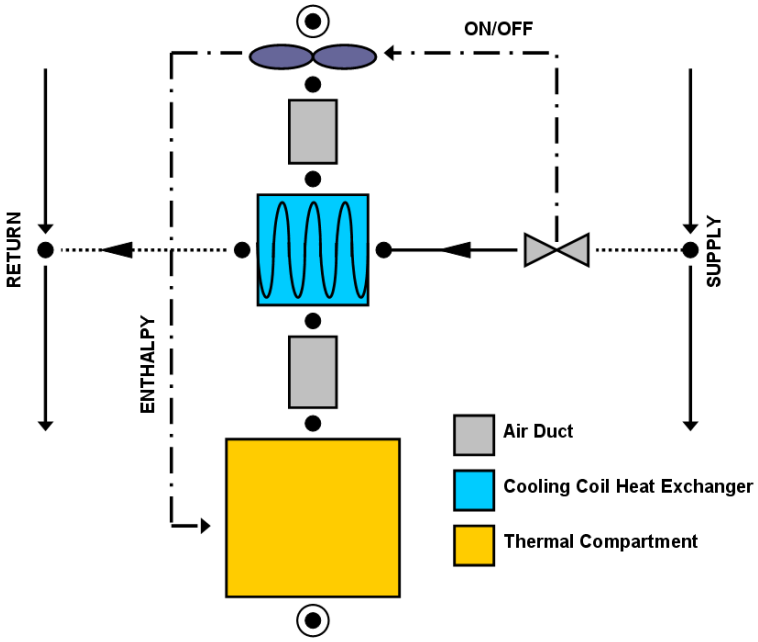

Figure 8: Constant-Air-Volume HVAC configuration in DTMS.

On/off control logic was implemented in DTMS to represent the nature of a CAV system. On/off control results in a metered variable fluctuating between user-specified high and low bounds. Specifically, a set point is established based on an enthalpy tolerance, thus, maintaining the compartment temperature within specified set points and between a set high and low range. For a seven-load network, on/off control results in the temperature behavior presented in Figure 9(a).

The effects of on/off valve control are immediately evident. For the control parameters specified here, after about 200 seconds of dynamic fluctuation, compartment temperatures settle into a regular oscillatory pattern with a period of approximately 280 seconds. The effect of closed chilled water valves is immediate; within tens of seconds based on the particular user-defined thermal load, the load temperature rises sharply to the maximum allowable bound. The effects of load placement are again significant. Loads 3, 5, and 7, the thermal loads of highest magnitude more than 10 m from the chiller, do not rise to the maximum temperature bound. This occurs because these valves are never set in the closed position; the on/off behavior of smaller and more proximate loads (1, 2, 4, and 6) is sufficient to keep higher magnitude loads within the specified temperature range. Figure 9(b) illustrates the fluctuation of evaporator heat transfer and shell-side liquid level, which are affected by the temperature behavior of return chilled water. After initial instabilities (where the controller for each load fluctuates between "open" and "closed"), these evaporator states reach an oscillatory equilibrium similar to that on the air-side of the simulation.

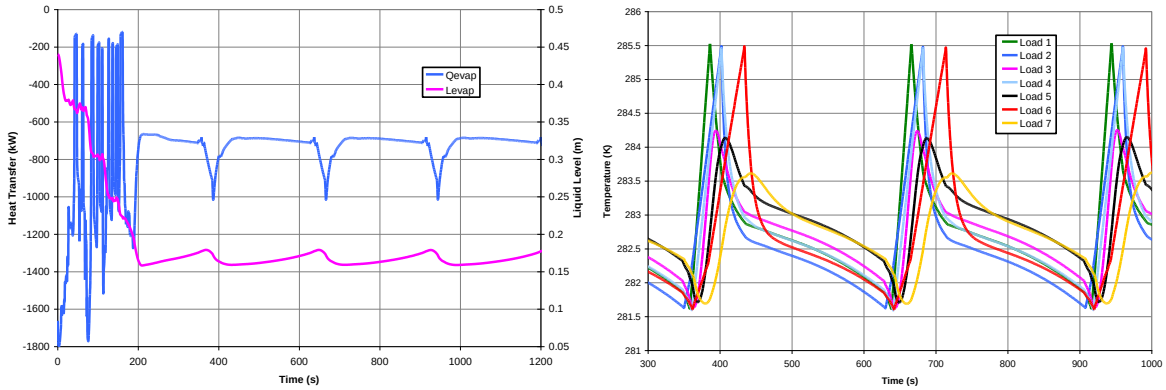

Figure 9: Results for a seven compartment cooling load with constant air flow:
(a) Compartment temperature (w/ 8 kJ/kg tolerance)
(b) Evaporator heat transfer and liquid level (w/ 8 kJ/kg tolerance).

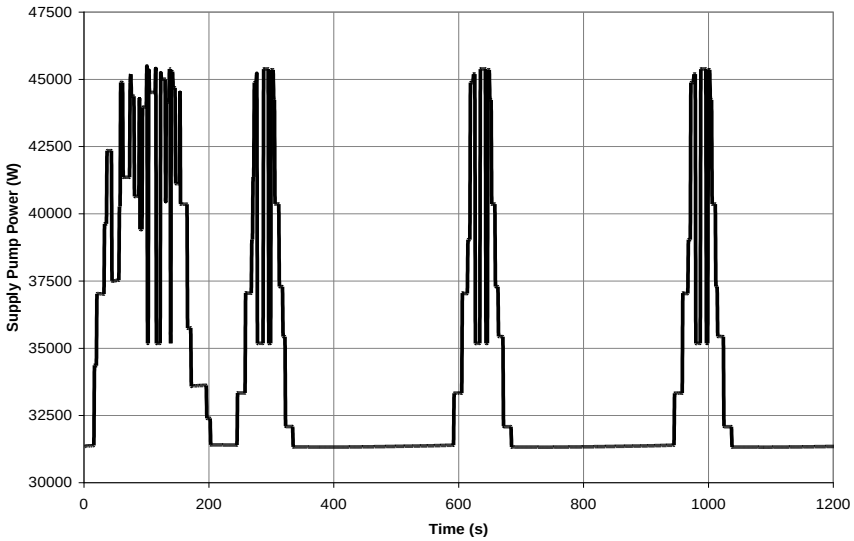

Figure 10: Supply pump power for a seven compartment cooling load with constant air flow.

Figure 10 illustrates the discrete nature of on/off control. The various plateaus of valve position combinations are apparent, especially in the first 200 seconds of transient behavior. Since oscillating valve conductance's impact the overall chilled water flow network, the supply pump oscillates between a peak value of about 45.4 kW, with all seven valves in the open position, and 31.3 kW with valves 1, 2, 4, and 6 closed.

Management of seven thermal loads while employing variable valve technology was simulated. Supply pump power requirements were compared with the CAV results to model anticipated power savings based on the utilization of variable-speed equipment. If the 8 kJ/kg tolerance (about 2^{o}C) of Figure 9 is retained, the variable-air-volume (VAV) supply pump consumes significantly less power in transporting chilled media to thermal loads. Referring to Figure 11, the 8 kJ/kg tolerance results in more than 16% power savings for the VAV chilled water supply pump and, presumably, for the variable-speed fans as well.

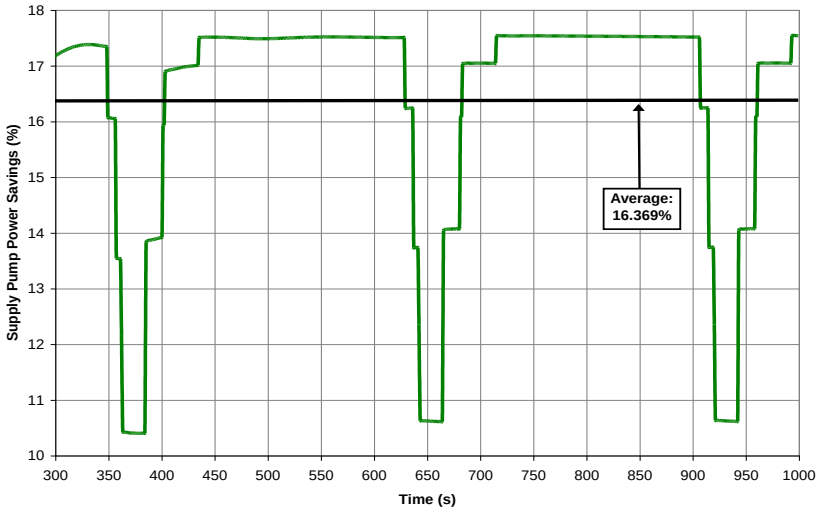

Figure 11: Supply pump power savings: VAV versus CAV in shipboard HVAC (retaining 8 kJ/kg tolerance).

To properly quantify these results in terms of anticipated fan power savings, power statistics on an existing shipboard configuration must be known. A total ship HVAC model corresponding to the DDG-51 class destroyer provides this fan data [15]. The power savings results of Figure 11 have been extrapolated in Table 1 to produce predictions for power savings based on the introduction of variable-speed fans.

Table 1: Anticipated fan power savings: VAV versus CAV shipboard HVAC

Tolerance [kJ/kg]	**Power Savings** [%]	**DDG-51 Fan Power** [kW]	**Total Fan Power Saved** [kW]
8.0	16.369	430	70.39

Conclusively, this advanced cooling strategy not only provides immediate power savings relative to the baseline, but also provides the potential for simulation of dynamic reconfiguration deemed necessary for future naval surface ships.

5.3 Thermo-Electric Co-Simulation of Power Conversion Systems

Pruske [13] built a model to link a shipboard electrical power system, and the consequent heat loads, into the DTMS framework. An electric power model, based on switch-averaged representations of three, advanced power converter modules (PCMs), was created to capture the transient nature of heat dissipation as a function of the dynamic nature of the electrical, power distribution network. These simulations were conducted for both air- and water-cooled module bays and included the US Navy standard DC-DC converter (PCM-1), DC-AC inverter (PCM-2), and AC-DC converter (PCM-4). As depicted in Figure 12, the power network was then integrated with a thermal resistive network linking the heat loads to the thermal management network. The resulting co-simulation is dynamic in nature and captures the essential transient characteristics of heat flow and energy storage while accommodating the greatly disparate time scales inherent to thermal and electrical networks.

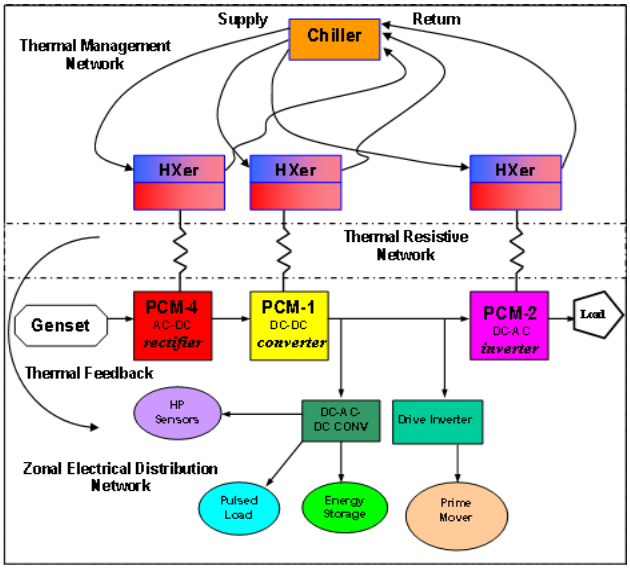

Figure 12: Thermal-electrical modeling in DTMS

For example, Figure 13 depicts the electrical configuration of the PCM-4. The PCM-4 is a transformer and 12-pulse, thyristor controlled, rectifier that steps down three-phase AC voltage from 4,160 V_{rms} to 500 V_{rms} at a frequency of 60 Hz, which is then converted to DC power at 1,000 V_{rms} by the rectifier bridge [16]. A wye transformer with a rating of 3 MVA performs three-phase AC voltage step down. A DC link capacitor with a parallel resistive load is used to mitigate voltage transients.

It was assumed that adequate electro-thermal co-simulation only requires electrical models that are sufficient to represent the longer term dynamics of electrical power conversion, i.e., from a thermal perspective it is not necessary to model the complex switching aspects of a converter as long as resistive and switching heat losses are adequately represented. Thus, an "averaged-switch model" was considered appropriate for simulating the dynamics of power conversion while simultaneously accounting for energy losses during the process.

Figure 14 is a representation of the modeling accommodations needed to simulate the PCM-4 using an averaged-switch model. To convert to an averaged-switch model, the PCM-4 requires two modifications. Obviously, the first is to use *rms* values of voltage rather than the actual three-phase sinusoidal voltage source. Use of *rms* values is illustrated in Figure 14, where the voltage source is labelled $V_{ac,rms}$. The second modification is to transform the switching elements into simple linear circuit elements. Thus, diodes and switches that compose the 12-pulse rectifier bridge are converted into current sinks and resistances, respectively. In this manner, the model is able to simulate the low frequency response of the system and bypass high frequency harmonics while still accurately representing overall behavior of the system [17].

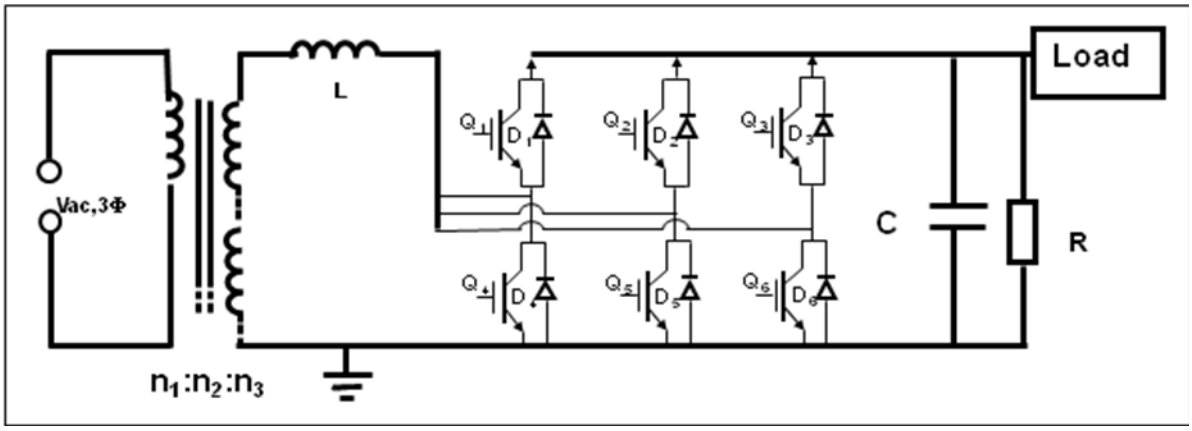

Figure 13: Electrical configuration of PCM-4 (for clarity, only 6 rectifier elements are shown).

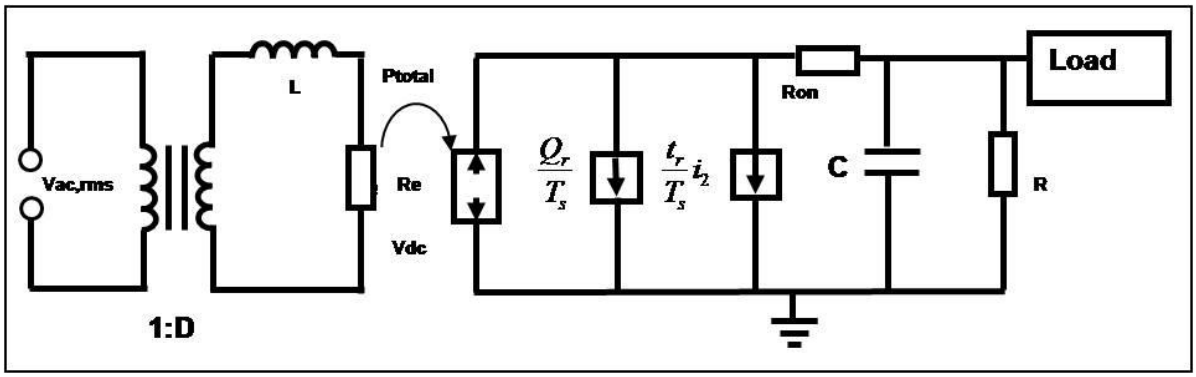

Figure 14: Averaged switch model of the PCM-4.

To demonstrate this model, an event simulating the behavior of the PCM-4 during a step change from part load to full rated power was constructed. Figure 15 shows the efficiency of the PCM-4 as simulated in DTMS. The step load occurs at 5 seconds and introduces a load at the rated capacity of 3 MW. The transient recovery time is approximately 0.015 seconds and the PCM-4 achieves a full load efficiency of about 96.2%. The PCM-1 and PCM-2 were handled in a similar manner as documented in [13]. To test the entire electrical distribution framework, a simulation was conducted with successful validation against results from the Zonal Electrical Distribution System (ZEDS) in the Naval Combat Survivability (NCS) Testbed [18].

Electrical circuit elements heat up during operation and their properties change as a function of local temperature. Heat losses associated with the resistor are termed Joule heating and are

characterized by:

$$P_{loss} = V^2 / R \tag{20}$$

where P is the power, V the voltage, and R the resistance. A resistor is used in a variety of DTMS models including resistive elements, switching losses, circuit breakers, resistive loads, and impedance.

The resistance is treated as temperature dependent and expressed as follows:

$$R = R_{ref}\left(1 + \alpha(T - T_{ref})\right) \tag{21}$$

where T is the local temperature, R_{ref} is the resistance at a reference temperature T_{ref}, and α is a constant based on material properties [19].

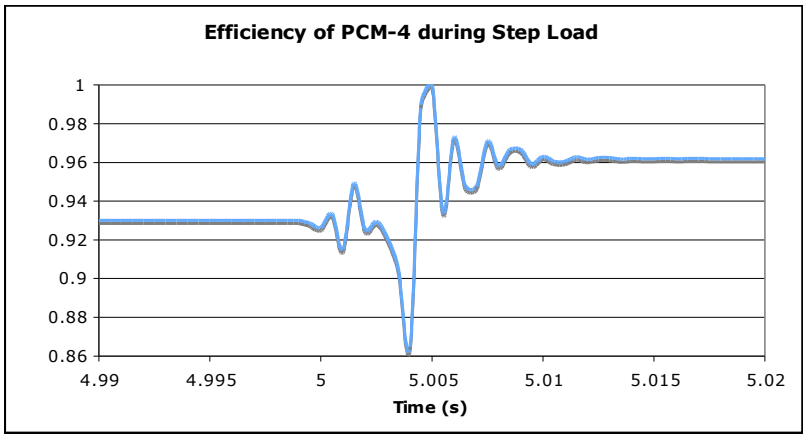

Figure 15: Efficiency of the PCM-4 during step loading, partial load to full load.

In accordance with the averaged-switch method, switches are modeled as a generic transistor and a diode with losses averaged over the switching time period. Switching losses in the diode are a combination of the removal of the recovered charge, Q_r, and the concurrent reverse recovery time, t_r [17]. Current losses associated with a diode during a switching event are then:

$$i_{loss}\big|_{T_s} = \frac{1}{T_s}\int_0^{T_s} i_1(t)dt = \frac{1}{T_s}\left(Q_r + t_r \cdot i_2\big|_{T_s}\right) \tag{22}$$

where T_s is the switching period, i_1 is the current of the diode in its on-state, and i_2 is the current in the transistor (the switch counterpart to the diode) in its on-state. The total power consumed by switching losses is then:

$$P_{sw} = V\left(\frac{Q_r}{T_s} + \frac{t_r}{T_s} \cdot i_2\big|_{T_s}\right) \tag{23}$$

Transistors block current during the off-state and conduct current during the on-state. During the off-state, the resistance of a transistor approaches infinity while during the on-state the transistor is said to have an on-resistance, R_{on} [17]. Thus, the current, i_T, through a transistor is modeled as:

$$i_T = \frac{V}{D \cdot R_{on}} \tag{24}$$

where D accounts for the duty cycle.

Transformer losses consist of core, eddy current, and winding losses. Losses via conduction through the core consist of sinusoidal hysteresis and eddy current losses. Temperature dependent hysteresis losses in the transformer core are modeled as follows:

$$P_{core} = k \cdot f^x B^y (aT^2 - bT + c) \tag{25}$$

where k is a constant based on the material, f is the frequency, B is the peak flux density, x identifies the frequency exponent, y the flux density exponent, and a, b, and c are constants. Eddy current losses per volume are expressed as a function of frequency and total flux as follows:

$$P_e = \frac{\pi^2 f^2 B_{\max}^2 a^2 \sigma^2}{6} \tag{26}$$

where a is the lamination thickness and σ is the thermal conductivity. Winding losses are caused by Joule heating and therefore, Equation 20 is appropriate to describe these losses.

Inductors exhibit losses in the form of winding losses and core losses. Winding losses consist of DC and AC losses. Conductive winding losses related to DC losses are similar to those of a resistor and are characterized by Equation 20. Core losses are associated with hysteresis and are characterized by the following expression:

$$P_{core} = k \cdot f^x B^y \cdot V_e \tag{27}$$

where V_e is the effective core volume.

Capacitance is also treated as temperature dependent in the PCM models. While this behavior is highly nonlinear at extreme temperatures, within a range of 20 to 100°C the relationship is linear for most dielectric materials [20]. In this range, the following expression is used to describe the temperature dependence [17]:

$$C = C_{ref}\left(1 + \beta(T - T_{ref})\right) \tag{28}$$

where C_{ref} is the capacitance at the reference temperature and β is a constant based on material properties. The temperature range of 20 to 100°C is considered adequate to cover the expected temperature range of shipboard converters.

In DTMS, the architecture of a cabinet bay of electronics employing forced convection consists of two networks: a fluid flow network and a heat flow network. Both air-based and liquid-based forced convection are accommodated. Figure 16 illustrates these two networks for the liquid-

based configuration as modeled in DTMS. The fluid flow network consists of an inlet source with a specified temperature and pressure, a pump to increase the pressure head, a mid-pressure node, a pipe, and an outlet with specified pressure. The heat flow network consists of an internal heat generation model, a boundary temperature node, a conduction model, and a boundary temperature node to model the temperature of the plenum.

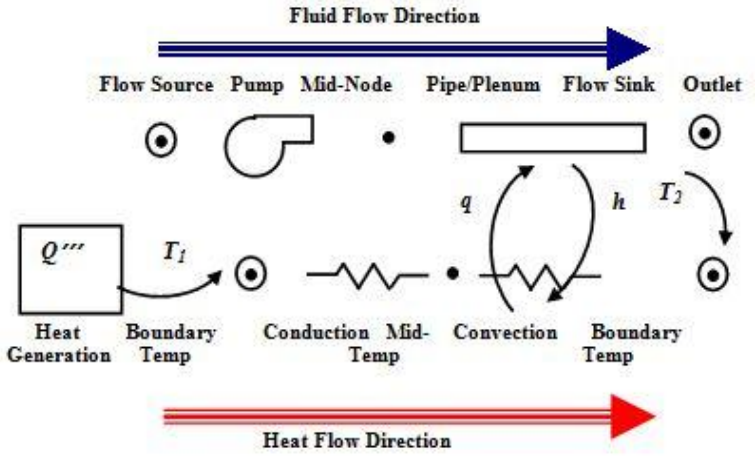

Figure 16: Cabinet bay model with fluid and heat flow networks.

A thermal resistive network was created in DTMS to simulate heat flux from PCMs. This network directly links heat dissipated in the electrical network to the thermal management network as depicted in Figure 12. Flow models are used to provide the solvers with the flow while temperatures are adjusted in the solver until flow models converge. Thus, flow models must provide the flow equation as a function of the temperature:

$$q'' = f(\Delta T) \tag{29}$$

This network is one-dimensional and captures the essential transient characteristics of heat flow and energy storage. The following standard relationships provide the convective and conductive heat flux, respectively:

$$q'' = h(\Delta T) \tag{30}$$

$$q'' = \frac{k}{L}(\Delta T) \tag{31}$$

where h is the convective heat transfer coefficient, k is thermal conductivity, L is a characteristic length through a solid surface, and ΔT is the temperature difference for heat transfer. The model can be employed in a conductive and/or convective environment depending on user input. Various arrays of fins on a flat plate are also capable of being simulated. Pipe and duct flow models are used to simulate removal of heat from either a heat sink or fin array, respectively.

An internal heat generation model was specifically created to satisfy the need to simulate heat generation and energy storage in electrical components. The heat equation for a finite volume within a solid experiencing energy storage and energy generation in one spatial dimension is as

follows:

$$\frac{1}{\alpha}\frac{\partial T}{\partial t} = \frac{\partial^2 T}{\partial x^2} + \frac{q_{vol}}{k} \tag{32}$$

where α is thermal diffusivity and q_{vol} is the volumetric internal heat generation. In DTMS, this equation is solved numerically using finite difference approximations.

The three flow networks (fluid, thermal, and electrical) were linked for the purpose of conducting dynamic, thermal-electrical, co-simulations. The intent was to investigate the importance of temperature dependency in the electrical models during feedback between the fluid, heat, and electrical flow networks. The next few paragraphs address the impact of thermal effects by presenting simulations of PCM efficiencies, bulk loads, and temperature transience without thermal dependency and then comparing these using a simulation, of the same configuration, with thermal dependency.

The configuration for this simulation, shown in Figure 17, consists of a PCM-1 converting and providing DC power to a PCM-2 for further conversion to AC power. The converters are initially operating at a partial load of 2.5 kW. This creates heat loads of 85 and 135 W for the PCM-1 and PCM-2, respectively. These loads have an insignificant effect on temperature of the electronics, and the thermal management network is able to maintain the converters within one degree Celsius of the starting temperature of 44°C, the temperature of the forced air [21] in this case. The PCM-1 and PCM-2 are then subjected to a load of 100 kW after an arbitrary time of 30 seconds at partial load. Total simulation time is 7200 seconds and air flow rates are 0.052 and 0.182 kg/s for the PCM-1 and PCM-2, respectively. These flow rates conform to those reported in [21]. The PCM-4 is not included because data regarding its geometry and thermal management are not available. Multi-zone simulations were performed, but are not reported here due to space limitations.

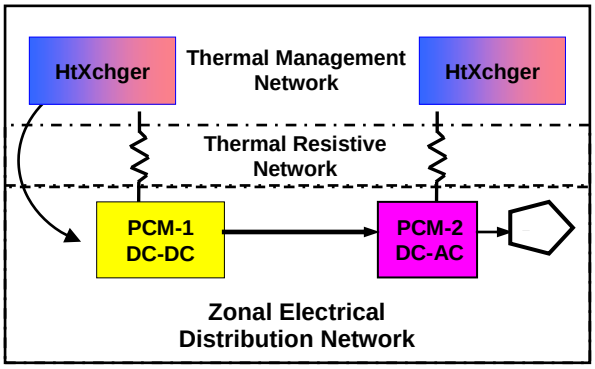

Figure 17: PCM configuration used to test thermal dependency of the converters.

Figure 18 shows the efficiency and bulk internal temperature of the air cooled PCM-1 and PCM-2 during the first 30 minutes and 66 minutes of operation, respectively. Both are thermally dependent cases. As expected, these figures indicate a steady decline in efficiency as the temperature within the bays of each cabinet increases. The bulk internal temperature of the electronics in the PCM-1 reaches the threshold value of 100°C within 27 minutes. At this critical

temperature, efficiency has dropped from 95.6 to 95.1%. The PCM-2 reaches 100°C within 67 minutes. At this time, the efficiency has dropped from 96.3 to 95.8%. In comparison, during the non-thermally dependent case, the PCM-1 and PCM-2 maintain a steady-state efficiency of 95.6 and 96.3%, respectively, while reaching 100°C within 30 minutes and 74 minutes, respectively. Figure 19 shows the bulk heat load of the PCM-1 and PCM-2 during this simulation.

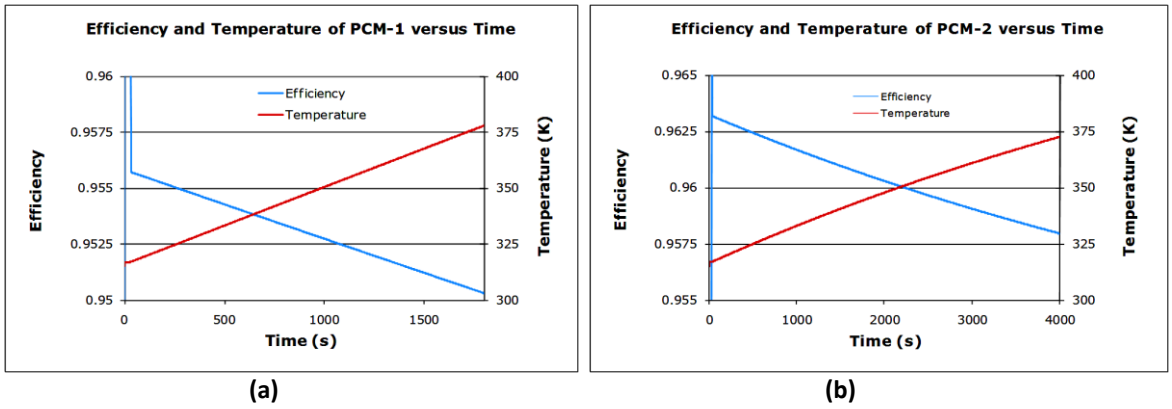

(a) (b)

Figure 18: Efficiency and temperature of air cooled PCM-1 and PCM-2 during operation.

While a 0.5% drop in converter efficiency may seem insignificant, these efficiencies compound to create significant losses at a system-level. For example, if 9 MW of rated power from a generator were converted from AC to DC (in a PCM-4), high voltage DC to low voltage DC (in a PCM-1), and finally DC to AC (in a PCM-2), and if the PCM-4, PCM-1, and PCM-2 were all operating at 100°C, this lower efficiency would create an additional 135 kW of waste heat, requiring more than 38 tons of capacity for active chilling.

By increasing the air flow rate in the thermally dependent case, a condition that maintains the converters below 100°C can be found. Increased airflow rates of 0.22 and 0.2 kg/s for the PCM-1 and PCM-2, respectively, produce the results shown in Figure 20. With this increase in airflow rate, the PCM-1 and PCM-2 fans must increase their power usage by 400 W and 280 W, respectively. Energy saved by increasing the airflow rate and maintaining a higher efficiency is 55 and 10 W for the PCM-1 and PCM-2, respectively. Thus, maintaining the converters at a lower temperature does not result in greater system-level efficiency.

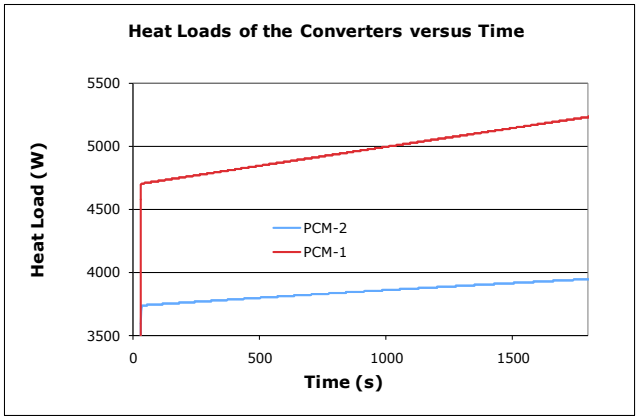

Figure 19: Heat loads (W) of air cooled converters during conversion of 100 kW.

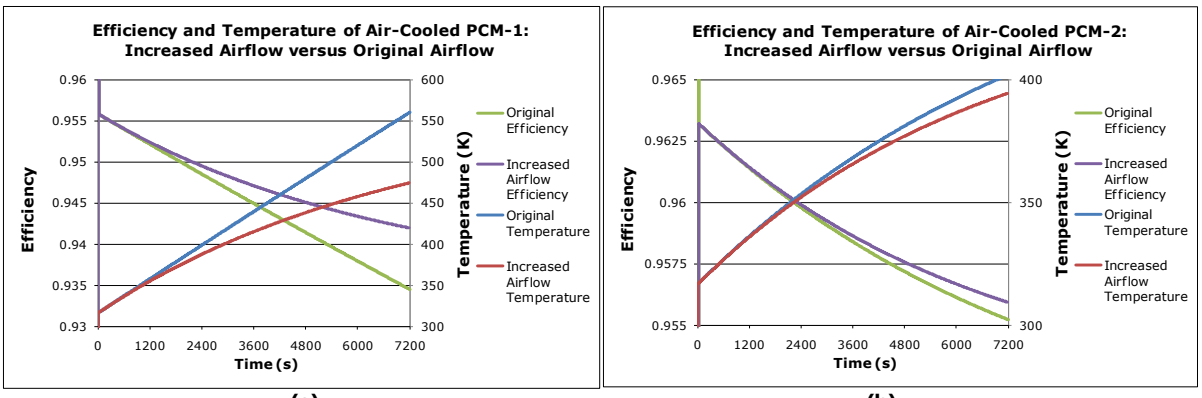

(a) (b)

Figure 20: Efficiency and temperature of PCM-1 and PCM-2 with original versus increased airflow rates.

Cooling of PCM electronics using liquid forced convection is an attractive alternative. In the following simulations, the configuration is identical to that discussed previously. However, the electronics are now cooled by direct, water-based convection using chilled water at 6.6°C with a flow rate of 1.39 kg/s pumped through a conduit in direct contact with the thermal heat sink. The flow rates reflect values suggested in Zerby, et al. [22].

Figure 21 compares the bulk internal temperature and efficiency of electronics in water cooled converters with those of the air cooled converters presented previously. As expected, forced convection of water removes heat at a rate much greater than the forced convection of air. The efficiency of each converter reflects the temperature behavior. Clearly, the Navy must continue to consider alternate cooling means, such as direct chilled water or phase change and immersion cooling, to address the much greater future heat loads expected in cabinets such as these.

A PCM experiences a duty cycle based on mission requirements. Thus, they are not typically operated at full capacity for indefinite periods of time. To demonstrate behaviors under discreet, time dependent loads, a simulation was conducted using a configuration like that above, but with multiple "events" listed in Table 2 below. Figure 22 shows the transient temperatures in the PCM-1 (converter is SSCM) and PCM-2 (inverter is SSIM) during this scenario. Not surprisingly, it is evident from the figure that the greatest rate of temperature increase corresponds to periods of operation at full capacity. Also, it is evident that the periods of operating at partial load do not require cooling water flow rates as high as 1.39 kg/s.

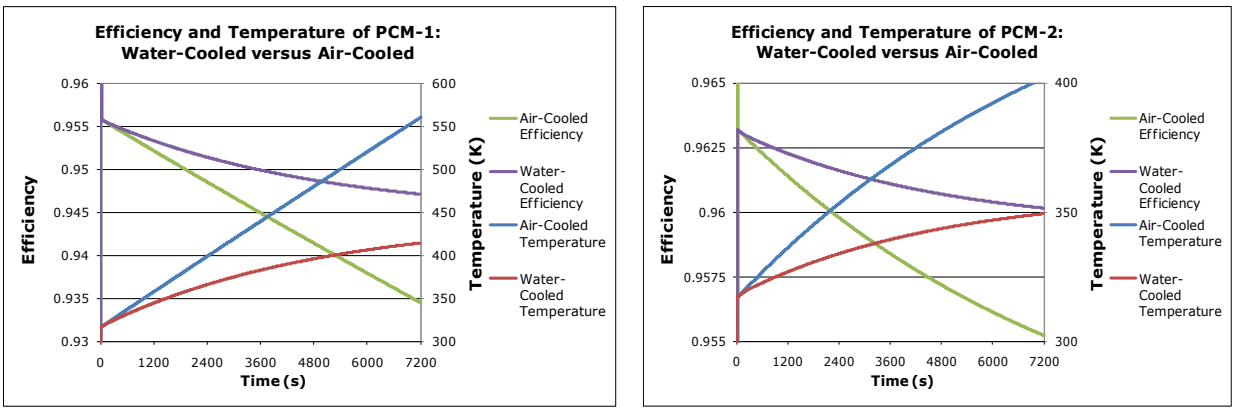

(a) (b)

Figure 21: Temperature and efficiency of water cooled vs. air cooled PCM-1 and PCM-2.

Table 2: Time and event loads for water-cooled converter simulation.

Time (s)	Load (kW)
0	2.5
3	100
1800	10
3600	2.5
7200	10
18000	100
19800	2.5

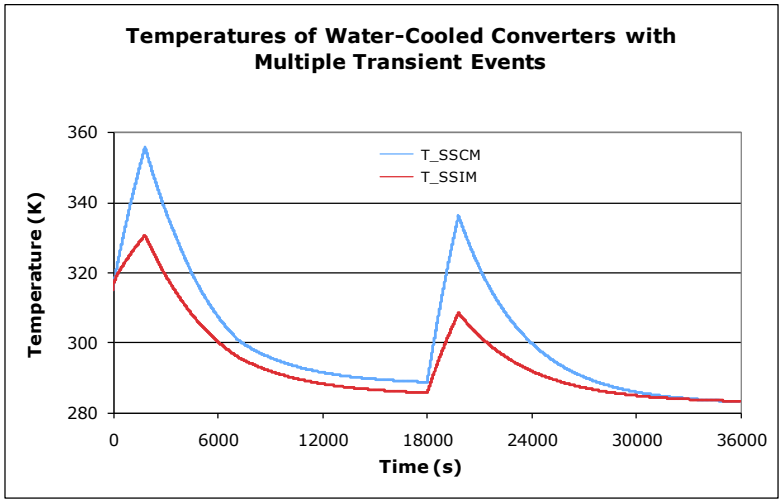

Figure 22: Temperatures of water cooled modules during several transient events (CM and IM).

5.4 Controls in DTMS

In the previous sections of this summary, a highly customizable simulation framework has been described and is capable of addressing thermal management issues across both the mechanical and electrical domains. The purpose of the current paragraph is to describe the introduction of

modern control theory into DTMS, thus, providing the framework with the ability to control large-scale, system-level simulations.

The research reported here simulates control of a marine chiller on the Arleigh-Burke class destroyer, similar in construct to the York 200-ton unit discussed in Section 5.2. The refrigerant flow in this machine is depicted in Figure 23. Several control strategies were implemented. These included the common proportional-integral-differential (PID) controller as well as a new controller based on optimal control theory. Results for chiller simulations in the case of no-control, PID control, and optimal control are presented here. Further details are reported in Salhotra [6].

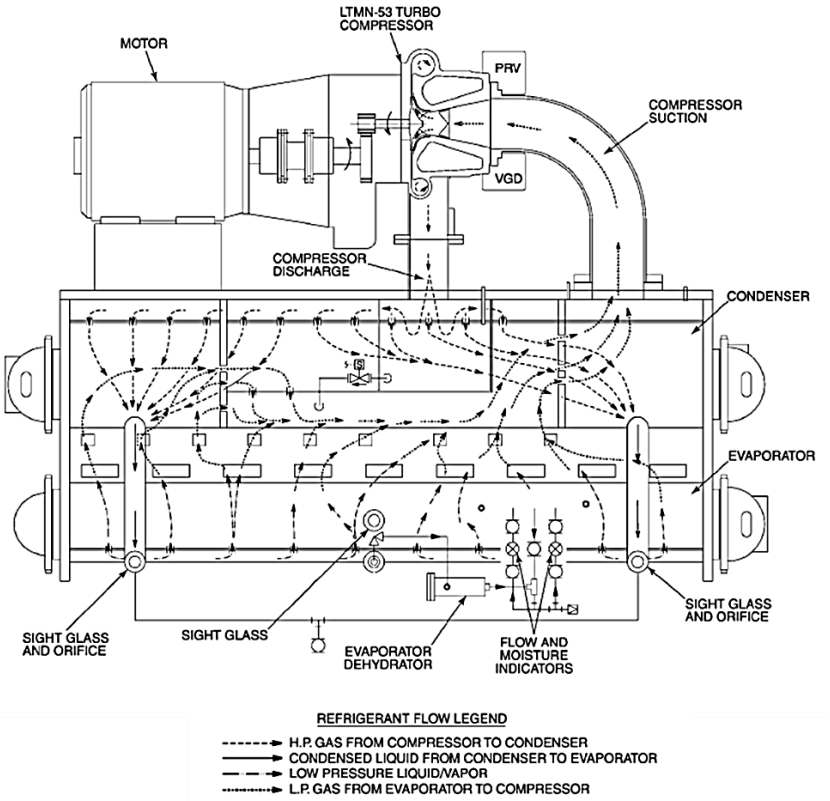

Figure 23: York 200-ton chiller with refrigerant flow diagram

PID control was originally modeled in DTMS [4] as a special case of a transfer function control scheme. A PID feedback control loop is based on controlling a single variable in the system to cause it to reach a pre-defined set point. It does so by subtracting the actual value of the variable from that of a set point to obtain an error. Based on the value of this error, adjustments are made to provide a control output u(t). The control output is a variable that can be manipulated by the user in the actual system. It does so by using three constants, the proportional gain (k_p), the derivative time constant (τ_d), and the integral time constant (τ_i):

$$u(t) = k_p e(t) + k_p \tau_d \frac{de(t)}{dt} + \frac{k_p}{\tau_i} \int e(t)\, \mathrm{d}t \qquad (33)$$

Manipulation of these parameters determines the control output and the eventual response of the variable being controlled. There is no general algorithm to access system variables and produce control outputs. In addition, these controls are clearly not independent of one another; changing one gain will change the effect of the other two. For example, reducing the proportional control may slow the system response and avoid large fluctuations of error with respect to time. In this case, the effect of derivative control, which works on the slope of the error with time as an input, would be diminished.

PID feedback is, by its very nature, local since it depends on the error between a given variable and its set point, regardless of the actual system dynamics. Achieving the objective of a single PID loop may create an undesirable effect in another part of the system, and multiple PID loops may well conflict. This can lead to instabilities that prevent the system from reaching a true steady state. Previous methodologies in DTMS included creating primary and secondary PID loops [4]. In this situation, the primary loop is active while the secondary loop is inactive. When the primary loop has maintained its monitored variable within the tolerance limit of its set point for a few time steps, the two controllers switch roles and the new primary controller becomes active. In this "leapfrog" methodology of control, two variables may fluctuate about their respective set points. Introduction of additional PID control loops would complicate this behavior and potentially render this approach totally ineffective. To deal with a complicated component such as a chiller with its multiple controls, it was found necessary to do away with the strategy of implementing localized PID loops and explore other options.

To overcome the above issues, the optimal control problem has been modeled in DTMS as an Infinite Horizon Linear Quadratic Regulator (LQR) problem. In the LQR formulation, a system-level control model computes outputs in a manner that takes into account contrasting effects of various outputs. This formulation is global, not local, and therefore, will create desirable effects in parts of the system that are not controlled directly by controller inputs. This strategy employs the state equations of the system as a whole, thus, taking into consideration all components and their resulting interactions. The principal advantage of this approach lies in calculating control outputs by quantifying changes in various parameters due to inter-component interactions as well as component-specific behaviors. Specific steps required to formulate the LQR problem are presented below.

In what follows, results of the LQR control strategy are shown and compared with chiller simulation results using both no-control and PID control cases. A schematic of the York 200-ton marine chiller configuration (with the hot gas bypass, heat load, and secondary fluid loops included) is shown in Figure 24. For reference, inlet and outlet states have been labeled for each device in the system. To determine the minimum number of critical states for the chiller, the interaction of various parameters at each of the 12 state points were studied to establish which variables change dynamically with respect to each other and which variables are static, time-invariant functions of others. In addition, "critical states" must be selected. Details of this procedure and outcome are reported in Salhotra [6].

The hot gas bypass valve (HGBV) connects the condenser to the compressor to ensure a controlled level of superheat in the refrigerant entering the compressor. Implementation of the LQR controller was demonstrated for startup to steady-state of this chiller at full load. Treatment of the optimal controller ends with simulation of the chiller and its LQR controller under the influence of varying dynamic heat loads in a chilled water loop. The heat load variations examined have highly transient characteristics that affect the temperature of the fresh water entering the chiller, and refrigerant pressure and temperature in the evaporator.

In the refrigerant loop, two components are modeled dynamically: the condenser and the evaporator. The compressor and expansion valves are fast reacting and thus modeled as static. The states that describe the refrigerant at the inlet and exit of the heat exchangers (i.e., P_3, h_3, P_4, h_4, P_7, h_7, P_8 and h_8) are of specific interest. Varying heat load conditions change the refrigerant evaporation and condensation pressure, and therefore, the pressure range in the compressor, valves, and piping. Changing these, and the flow rate across any of the valves, changes the outputs of the Newton-Raphson solver used to calculate flows and pressures throughout the circuit. The four critical system states are P_7, h_4, h_8 and T_{10a}. These selections are not unique, but they do provide the simplest expressions for time derivatives of the system states. The derivative equations of these system states are a function of the system states and control inputs. However, these derivatives are highly non-linear. To use linear optimal control theory, it is necessary to linearize the system model about an equilibrium point. This process is presented in Salhotra [6].

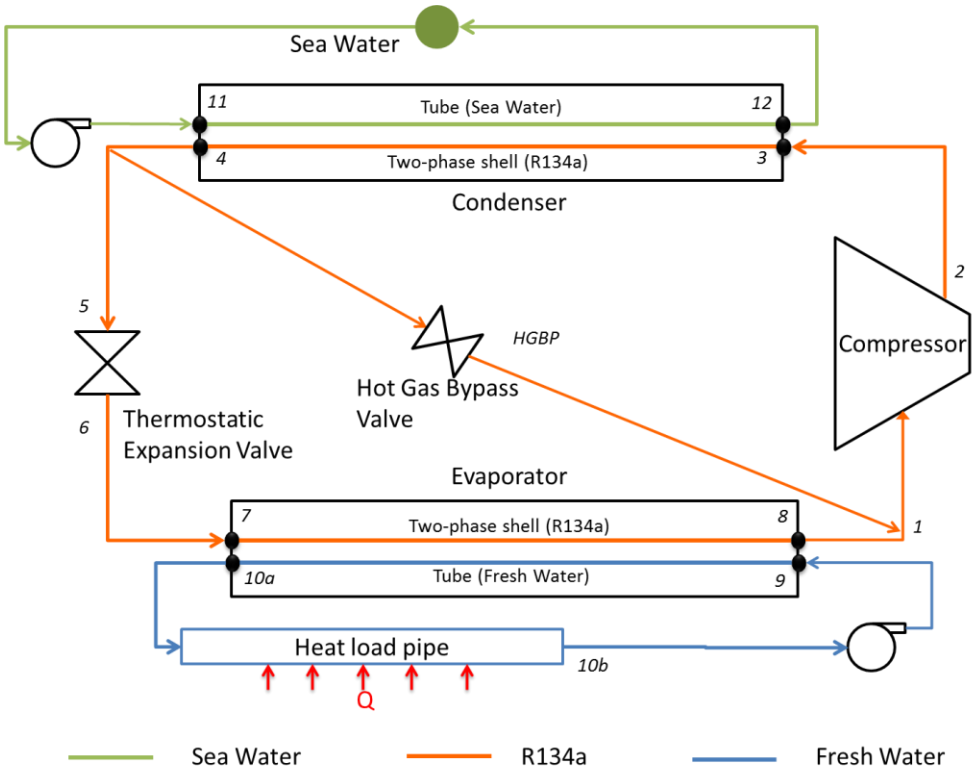

Figure 24: Schematic of the complete closed-loop chiller

Values of the control inputs and system states, which collectively describe the complete equilibrium system state, can be determined at full load. These are provided in Table 3.

Table 3: System states and inputs at *Heat Load* = 709.526 kW

Variable	Value (units)
P_7	328.603 (kPa)
h_4	132.0605 (kJ/kg)
h_8	252.294 (kJ/kg)
T_{10a}	279.82 (K)
n_{TEV}	71.2967 (% open)
n_{HGBP}	56.411 (% open)
$\omega_{CondPump}$	3888.3 (rpm)

In the table, n_{TEV} and n_{HGBP} are the thermostatic expansion valve and the hot gas bypass valve position, respectively, and $\omega_{CondPump}$ is the condensate pump speed.

To apply optimal control theory, a linearized model of the system about this equilibrium point is required. Define *X* to be the model state input vector, which is the difference between the system states and their equilibrium values. Similarly, define *U* to be a model control input vector, which is the difference between the system control inputs and their equilibrium values.

$$X = \begin{bmatrix} x_1 \\ x_2 \\ x_3 \\ x_4 \end{bmatrix} = \begin{bmatrix} P_7 - P_{7eqm} \\ h_4 - h_{4eqm} \\ h_8 - h_{8eqm} \\ T_{10a} - T_{10aeqm} \end{bmatrix} \tag{34}$$

$$U = \begin{bmatrix} u_1 \\ u_2 \\ u_3 \end{bmatrix} = \begin{bmatrix} n_{TEV} - n_{TEVeqm} \\ n_{HGBP} - n_{HGBPeqm} \\ \omega_{condpump} - \omega_{condpumpeqm} \end{bmatrix} \tag{35}$$

Note the difference between system states and control inputs (the variables on the right hand side in these expressions) versus model states and control inputs (the x_i and u_i). System states and inputs are physical variables in the chiller simulation, such as evaporation pressure (P_7) and thermostatic expansion valve position (n_{TEV}). Model states and inputs are the deviations of system states and inputs about their equilibrium point (x_1, u_1, etc.), and are used in the state-space formulation.

In linearized control theory, the derivative of the model states is expressed as a linear function of the model states and the model inputs, i.e.:

$$\dot{\boldsymbol{X}} = \boldsymbol{AX} + \boldsymbol{BU} \tag{36}$$

$$\frac{\boldsymbol{d}}{\boldsymbol{dt}}\begin{bmatrix}\boldsymbol{x_1}\\ \boldsymbol{x_2}\\ \boldsymbol{x_3}\\ \boldsymbol{x_4}\end{bmatrix} = \boldsymbol{A}\begin{bmatrix}\boldsymbol{x_1}\\ \boldsymbol{x_2}\\ \boldsymbol{x_3}\\ \boldsymbol{x_4}\end{bmatrix} + \boldsymbol{B}\begin{bmatrix}\boldsymbol{u_1}\\ \boldsymbol{u_2}\\ \boldsymbol{u_3}\end{bmatrix} \tag{37}$$

where *A* and *B* are constant coefficient matrices. To obtain linearized model equations, the system state derivative equations are reduced to functions of the system states and control inputs, and then linearized about an equilibrium point. This is known as the state-space representation of the system. Again the details of this development are presented in Salhotra [6].

The linearized system model clears the way to apply the principles of optimal control. Formulation of optimal control requires that an objective function (*J*) be minimized subject to system constraints. *J* is a scalar indicator of all system and control input deviations about equilibrium wherein appropriate weights are assigned to each input. In the case of optimal chiller control, the system must reach a defined equilibrium point at a steady-state, as determined by the heat load condition. This condition corresponds to all model states and model inputs approaching zero, i.e. $X_{ss} \rightarrow 0$ and $U_{ss} \rightarrow 0$ as $t \rightarrow \infty$. In the vocabulary of control engineering, this is called an "infinite horizon" problem. This condition is described by the following formulation of the objective function:

$$\boldsymbol{J} = \int_{\boldsymbol{0}}^{\infty} \left(\boldsymbol{X^T QX} + \boldsymbol{U^T RU}\right)\boldsymbol{dt} \tag{38}$$

where *X* and *U* are again the model state and model input vectors, respectively. The superscript *T* indicates a transpose of these vectors. *Q* and *R* are constant diagonal weighing matrices appropriate to the particular control application and are positive semi-definite and positive definite diagonal matrices, respectively. For the infinite horizon problem, these are constant matrices. The optimal control problem is then to:

$$\begin{aligned} &\boldsymbol{min\, J} = \int_{\boldsymbol{0}}^{\infty} (\boldsymbol{X^T QX} + \boldsymbol{U^T RU})\boldsymbol{dt} \\ &\boldsymbol{subject\ to}\ \ \dot{\boldsymbol{X}} = \boldsymbol{AX} + \boldsymbol{BU} \end{aligned} \tag{39}$$

Expanding the integrand in the expression for *J* above produces:

$$\boldsymbol{J} = \int_{\boldsymbol{0}}^{\infty} (\boldsymbol{\Sigma x_m^2 q_m} + \boldsymbol{\Sigma u_n^2 r_n})\boldsymbol{dt} \tag{40}$$

where q_m and r_n are the indexed diagonal elements of matrices *Q* and *R*, respectively. In this formulation, the integrand is a quadratic function of the linearized model states and inputs. Also, as mentioned earlier, the system reaches steady state as $t \rightarrow \infty$. Therefore, this formulation is called an Infinite Horizon Linear Quadratic Regulator (LQR) problem.

Since J is to be minimized, a higher value for the state-weighing factor (q_m) will ensure a smaller value for the corresponding model state (x_m). Similarly, a higher value for the input-weighing factor (r_n) will ensure a smaller value for the corresponding model input (u_n). Therefore, increasing the weighing factor for a particular model state or input implies more emphasis on that equilibrium value and ensures a lower steady-state error. In the case of the York chiller, the temperature of the fresh water exiting the evaporator (T_{10a}) is more important than the evaporation pressure (P_7), because the deviation in P_7 might be as much as 1-2 kPa and yet the system would be considered to be running smoothly. In contrast, a deviation in T_{10a} beyond 1-2 Kelvins would be a cause for concern. Thus, q_4 (corresponding to x_4 and T_{10a}) in this model is assigned a weighing factor about four orders of magnitude larger than q_1 (corresponding to x_1 and P_7).

Equation 39 describes the control formulation for the Infinite Horizon LQR problem. The optimal input (U^o) for this problem is expressed as:

$$\boldsymbol{U^o = -KX} \tag{41}$$

where the feedback gain matrix (K) is obtained by solving what is known as the differential Riccati equation. In mathematics, a Riccati equation is an ordinary differential equation that is quadratic in the unknown variable. In LQR theory, this equation is given by:

$$\boldsymbol{A^T S(t) + S(t)A - S(t)BR^{-1}B^T S(t) + Q = \frac{dS(t)}{dt}} \tag{42}$$

where $S(t)$ is called the Riccati matrix. Other quantities in this expression have already been defined. The Riccati equation is a purely mathematical formulation used to solve the minimization problem. Since ours is an infinite horizon problem, the right-hand side is zero at steady state, and this equation reduces to the algebraic Riccati equation:

$$\boldsymbol{A^T S_o + S_o A - S_o BR^{-1}B^T S_o + Q = 0} \tag{43}$$

where S_o is the steady-state Riccati matrix. The gain matrix may then be expressed as:

$$\boldsymbol{K = R^{-1}B^T S_o} \tag{44}$$

Equations 39, 41, and 42, describe the optimal control output based on the given system model. The model states may be calculated at any given time using the formulation for the four system states and the value of the feedback gain matrix (K). The control algorithm calculates U, and the three control outputs for TEV position, HGBP valve position, and condenser pump speed.

To extend this formulation to other heat load (HL) cases, the following steps must be performed. System linearization is again performed using the new value of HL. The user may then obtain the new equilibrium value for the system states and inputs by performing a PID simulation in DTMS, without changing the control parameters. Then with the new HL and new time constant variables and equilibrium values for system states and inputs, one may readily obtain a model linearized about the new equilibrium point. Finally, with the linearized model determined for a new heat load, the scalar objective function (J) is obtained to complete the LQR formulation. The weighing values contained in matrices Q and R remain unchanged since the importance of various states relative to each other remains the same. With that the matrices A, B, Q and R have

been obtained for the new equilibrium state, and may be used to calculate the new feedback gain matrix (*K)*. Using these steps, new feedback gain matrices may be determined for various heat load values. This has already been done and the logic is coded in DTMS class *ChillerOptimalControl.* In effect, the feedback matrix has been adjusted based on system conditions; this is known as "gain scheduling".

Thus, a procedure exists to linearize the system model, formulate the objective function, solve for the steady-state feedback gain matrix, and design the optimal controller. On occasion, the linearized model may work for other circumstances, depending on response sensitivity to various conditions, and gain scheduling may not be required. Some control formulations in DTMS may require outputs to have a defined variation over time (called the "tracking problem"). In essence, model-based design of the controller handles each problem according to the characteristics of that problem, i.e., the problem at hand determines the procedures used to design the controller. Therefore, it is important for the control designer to have specific knowledge of optimal control theory, as applied to the particular model under control, before implementing this procedure for controller design.

Results obtained by applying the LQR controller formulation to the York 200-ton chiller in a DTMS simulation are presented and briefly discussed below. To assist the reader, PID and no-control responses are directly co-plotted with the optimal control results for comparison purposes. In the graphics that follow, these control responses are color-coded in blue, green, and red, respectively.

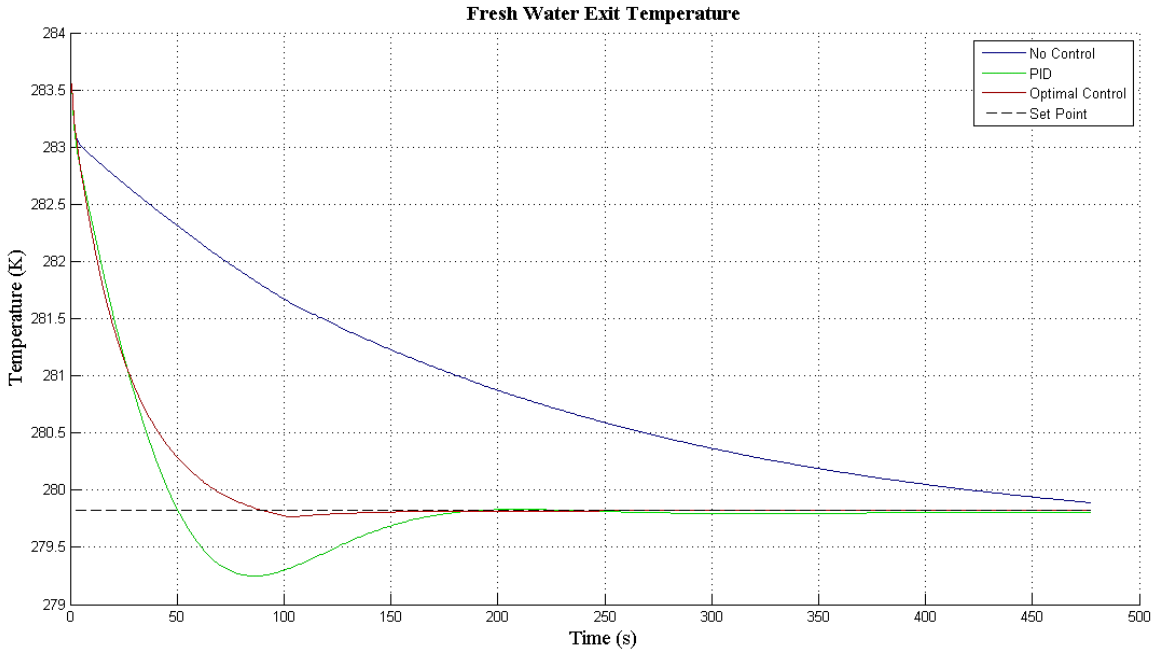

Figure 25 shows the time response for the fresh water exit temperature in the evaporator (T_{10a}) – the most important monitored variable in these simulations. In all three cases, but not apparent in the figures, there is a spike in the first few seconds of the simulation due to numerical startup response. This affect is caused by adjustment to initial conditions internal to the solver. In the figure, it is observed that the no-control simulation falls slowly to the steady-state condition over

a lengthy period exceeding 500 seconds, a number which is dependent on the system dynamics. Undershoot is observed in the case of the PID controller in the first 100 seconds. This behavior is absent in the case of optimal controller, even though both are approaching the set point at a similar rate. The PID undershoot may be reduced by increasing derivative control. However, this ploy would have the negative effect of producing larger steady-state time response and a larger settling time. Undershoot using the optimal controller is negligible. This occurs in a physical sense because the controller is aware of, and able to adjust to, all critical system states throughout the simulation.

Figure 26 shows the time response of the pressure in the evaporator for this simulation. As with the fresh water temperature, the evaporation pressure slowly falls to the equilibrium value in the case of no-control. The optimal control, once again, has a negligible undershoot and faster time response compared to the PID control, which again has a significant undershoot and an extended settling time.

Control outputs for the TEV, HGBP valve, and the condenser pump for all three cases are shown in

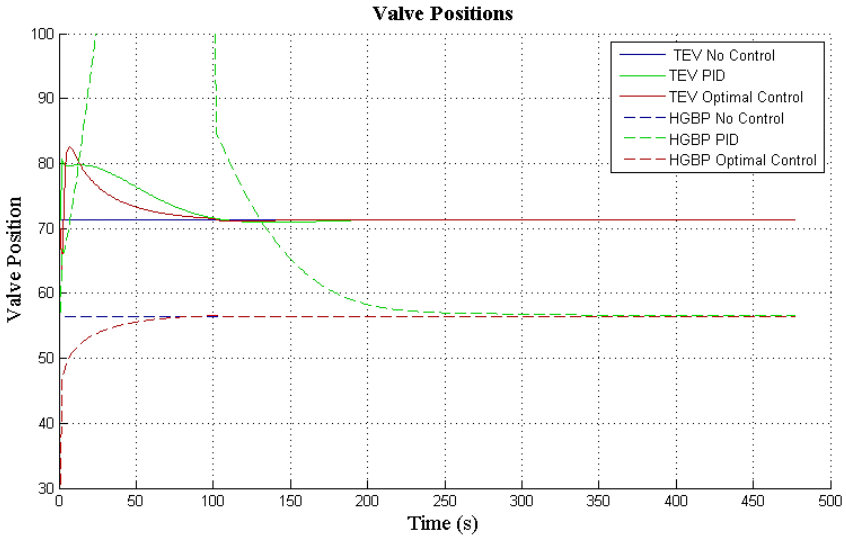

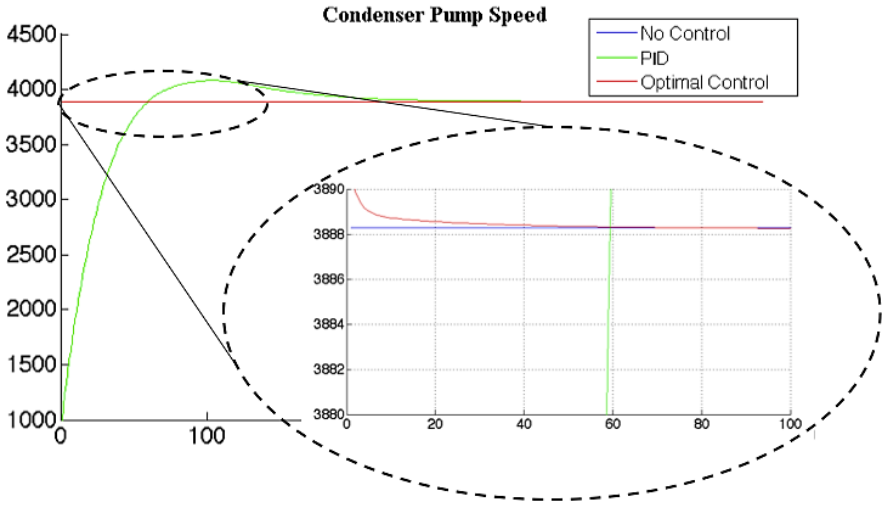

Figure 27 and Figure 28. The control outputs for no-control are maintained constant since none of the control

parameters are manipulated in this case. In contrast, there are significant fluctuations in the valve positions for the PID case; the changes in control parameters in this case are large enough to cause extreme and prolonged control outputs. In fact, the HGBP valve control spikes at about 25 seconds and remains fully open for approximately 75 seconds. Adjusting the overall PID control parameters might reduce this fluctuation, but this would also influence the overall settling time for the system. Significant variation in optimal controller output occurs in the first few seconds when numerical fluctuations dominate. The response then quickly settles to equilibrium conditions in a well-behaved manner. In both cases, TEV control outputs are better behaved than HGBP valve response.

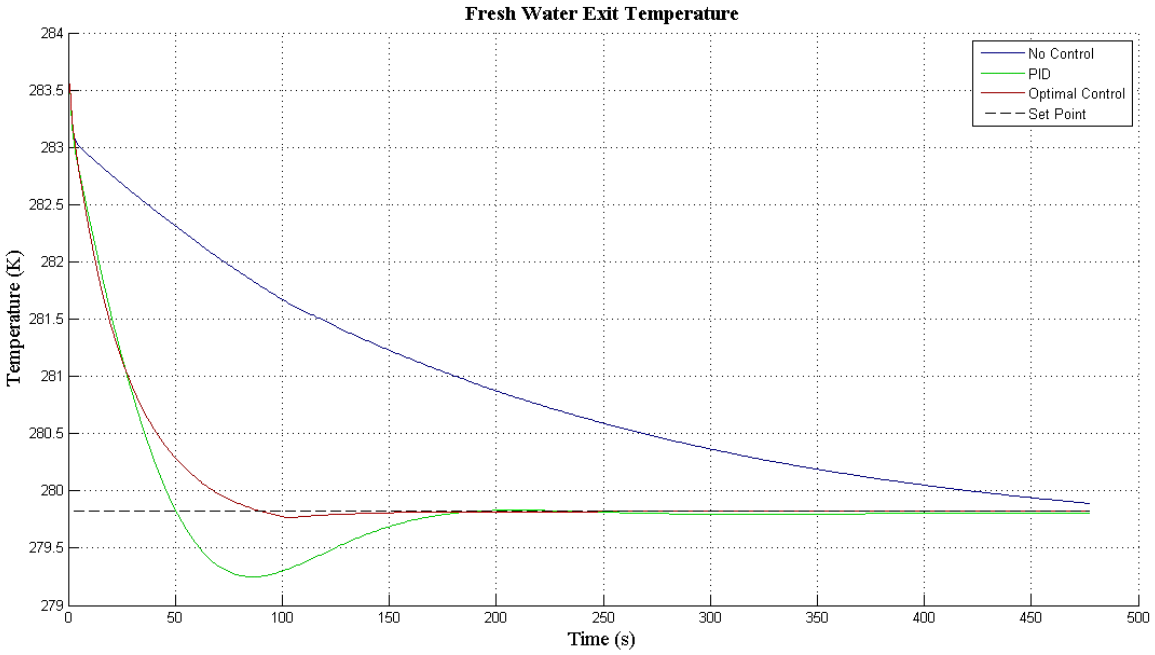

Figure 25: Fresh water temperature response for PID, Optimal, and No-Control

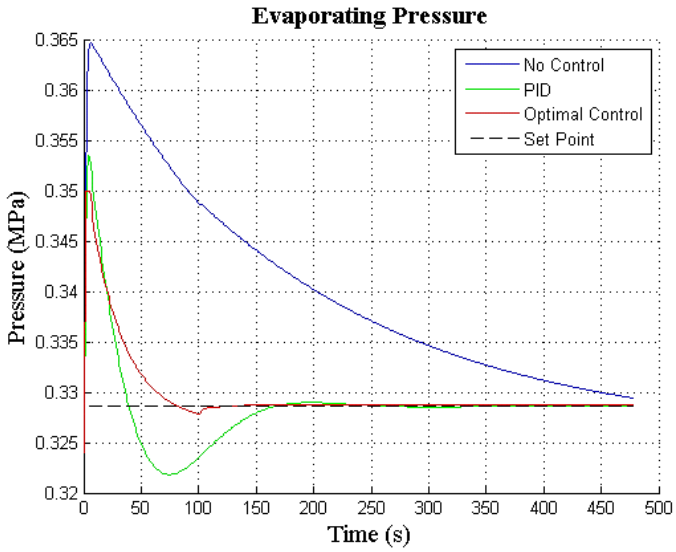

Figure 26: Comparison of evaporation pressure for PID, Optimal, and No-Control

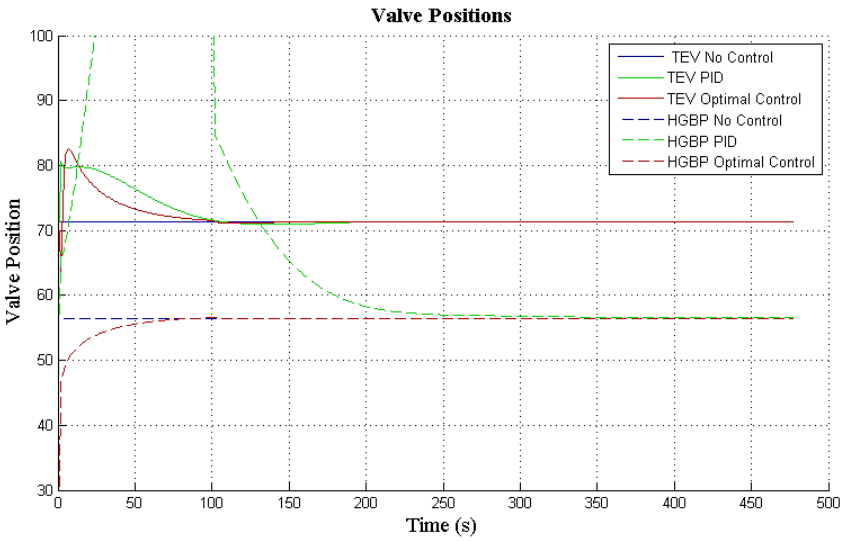

Figure 27: Comparison of valve position for PID, Optimal, and No-Control

A similar behavior is seen in

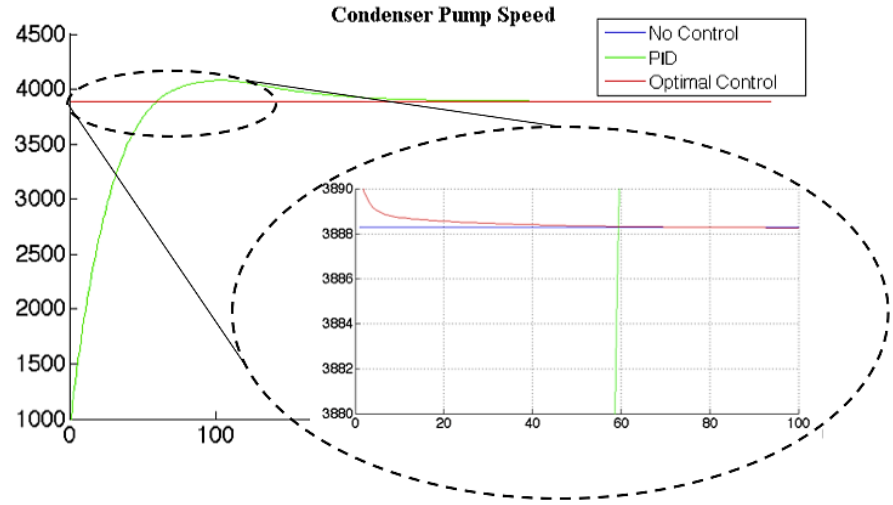

Figure 28, which displays the time response of the condenser pump speed to controller inputs. Recall that the equilibrium speed is 3888.3 rpm. In the PID case, the pump speed ramps up from about 1000 rpm. This occurs because the PID speed controller only monitors the exit enthalpy of the condenser shell (h_4). Initially, this enthalpy is significantly different from its equilibrium value, because the initial refrigerant condition is that of the compressor inlet. This significant negative error causes a control output that lies at the extreme of the pump speed range. As h_4 approaches equilibrium, so does the speed of the pump, with a significant overshoot and slow response time. In contrast to this behavior, the speed output in the optimal control case is based on all four state errors. At the initial condition the error in h_4 is large, but the errors in P_7, h_8, and T_{10a} are small. Also, h_4 is assigned less weight than T_{10a}, which further reduces its influence on the output. Therefore, the model output for the pump response (u_3) is small and the speed hovers around the equilibrium point as indicated in the inset oval.

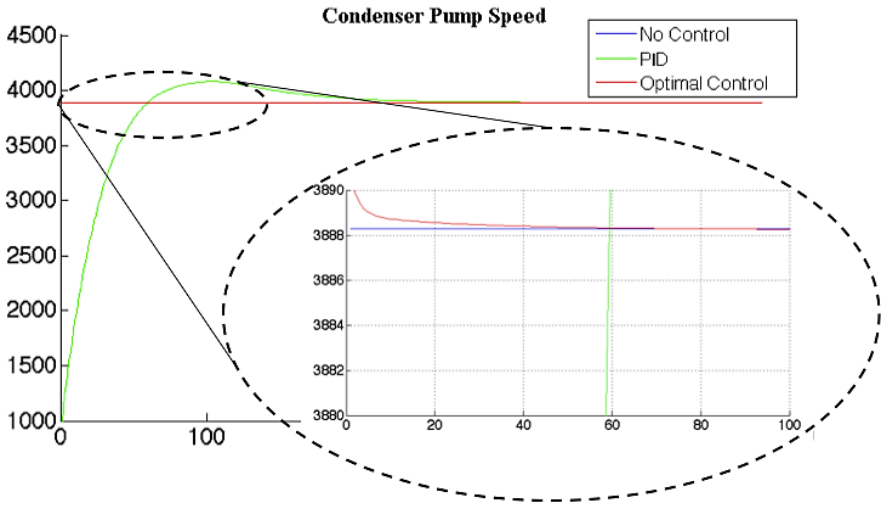

Figure 28: Comparison of condenser pump speed for PID, Optimal, and No-Control

Clearly optimal control is a significant improvement over PID control. The most important advantage of optimal control over PID is the global view that the controller has of the linearized system behavior. As a result,, the optimal controller is able to predict and minimize undesirable control outputs to elements of the system that are seemingly distant from the effect of that output. Unlike PID control, the LQR formulation takes into account all system parameters and interactions to provide control outputs that do not cause undesirable effects in parts of the system not directly controlled.

We next turned our attention to the ability of the LQR formulation to control the system and provide chilled fresh water at the evaporator tube exit under varying, dynamic, heat load conditions. Figure 29 shows the time varying heat load in the fresh water loop used in these simulations. The figure also shows the time varying heat exchange response to this load in the evaporator. During the 500 seconds of simulation, the heat load starts at 550 kW, increases to 700 kW (98.6% load), and then decreases to 530 kW (74.7% load). After an initial transient, the actual heat exchanged in the evaporator closely tracks the variation in heat load. The initial transient is a numerical artifact caused by the initial condition of saturated vapor at the evaporator shell inlet. As the shell inlet condition approaches the equilibrium value, it is clearly able to closely follow the time varying heat load. The response time to each step in heat load varies and slight overshoots as well as undershoots are observed.

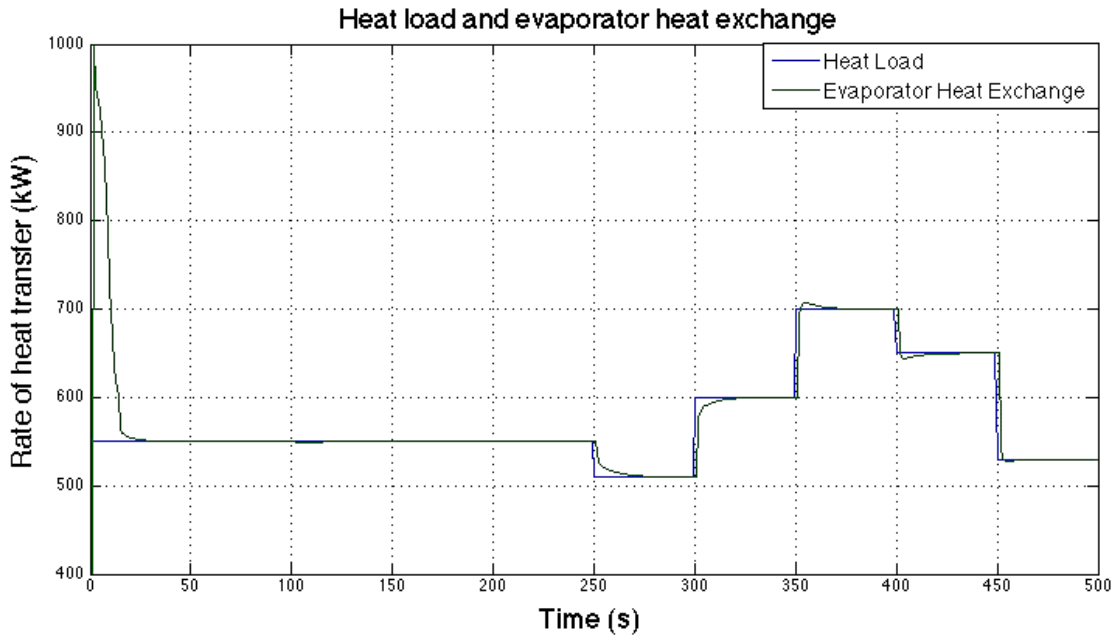

Figure 29: Variation of heat load and evaporator response with time.

The variations of component exit enthalpies with respect to time are shown in

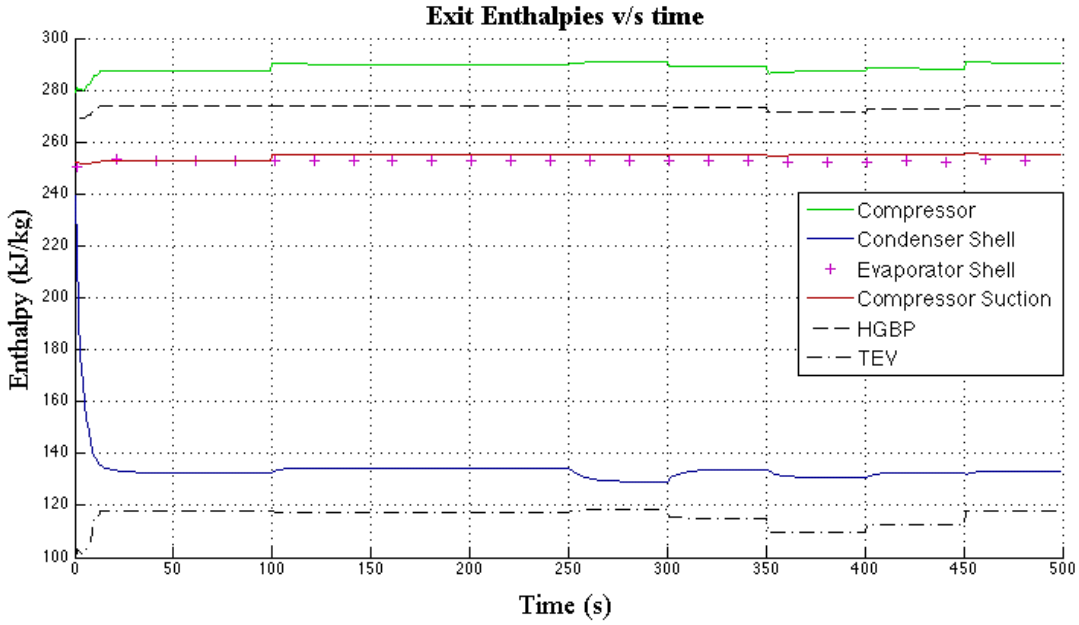

Figure **30**. Since they are modeled dynamically, the heat exchanger enthalpies vary smoothly in response to the changing load. Also, notice the nearly constant value of the compressor suction enthalpy, which is directly controlled by the HGBP valve to give a superheat of 3-5 kJ/kg (or 3-5 K) over the saturated vapor condition. Components such as the TEV, HGBP valve and compressor have small but sudden changes in their enthalpy as the heat load varies. This is because they are not modeled dynamically and, as a result, their exit enthalpies change almost instantaneously.

Figure 31 shows the variation of the evaporator fluid temperatures on the shell-side (refrigerant) and tube-side (fresh water). The fresh water exit temperature is a critical system state, and is given the highest preference to reach equilibrium by the LQR controller. Thus, its value remains nearly constant even though the fresh water inlet temperature varies considerably based on the varying heat load condition. The evaporator inlet temperature responds as the fresh water inlet temperature changes in order to minimize the variation of fresh water exit temperature. The evaporation pressure also changes with the evaporation temperature; this variation is shown in Figure 32.

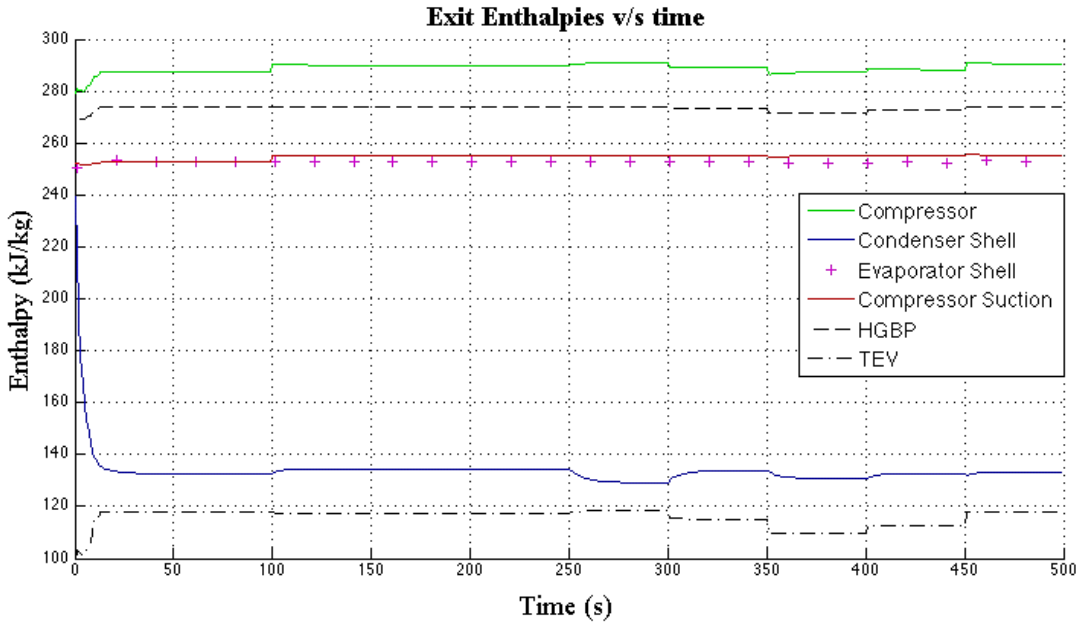

Figure 30: Variation of exit enthalpies with time.

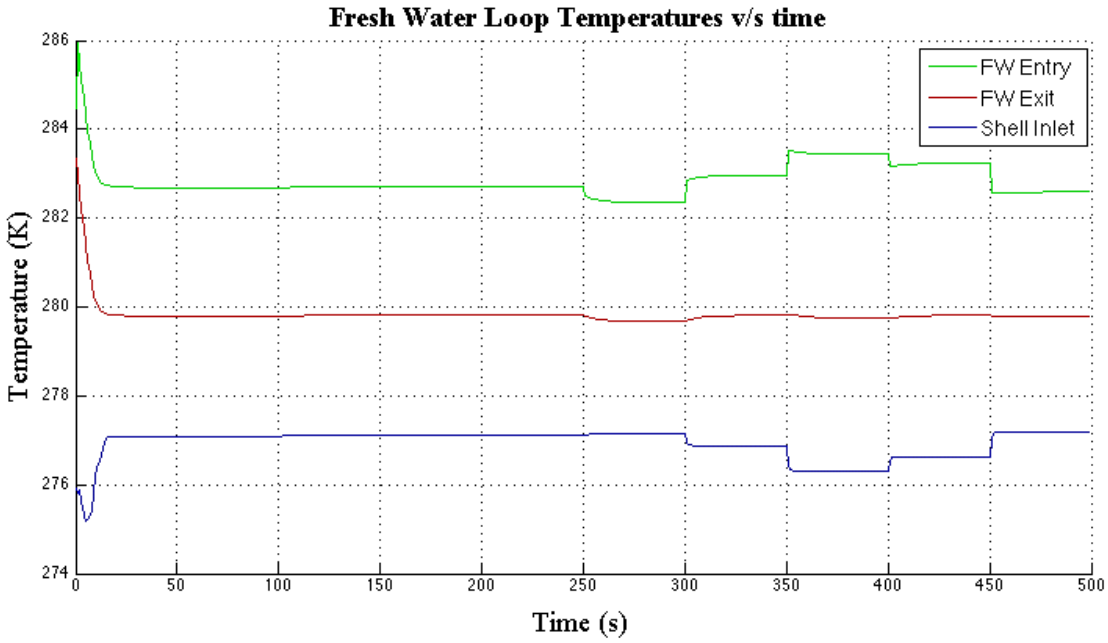

Figure 31: Variation of evaporator temperatures with time.

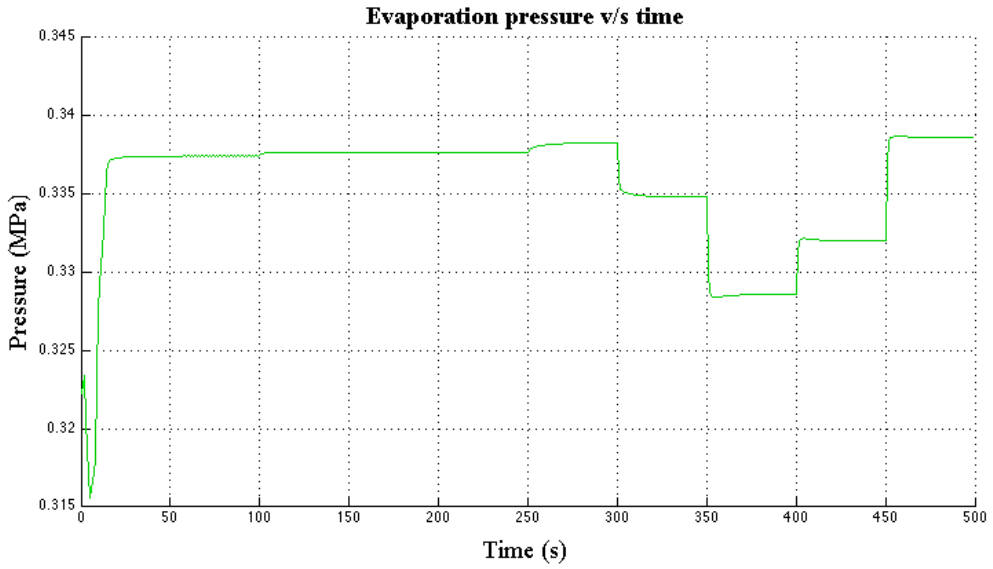

Figure 32: Variation of evaporation pressures with time.

LQR is a model-based controller design methodology, and thus, one must redo the entire procedure if a controller is to be designed for another system, or perhaps even the same system about a significantly different equilibrium point. Also, if the system is highly non-linear, then linearization may not provide the best results, unless models are built for multiple equilibrium points around a region of non-linearity. Thirdly, this system does not account for disturbances of any kind. In reality, disturbances are inherently present in every system, and controlling the

system in their presence is critical. These and other issues are addressed in more advanced control theories, such as Model Predictive Control.

6 CONCLUSIONS

This summary report describes a general purpose simulation tool, the DTMS framework, that was specifically created to address the US Navy's need for design-oriented characterization of thermal interactions with high power, mechanical-electrical components notionally planned for their future all-electric ships. The paper also summarizes several examples where DTMS is used in system-level simulations, e.g., an AES integrated electric propulsion system, chiller-based management of shipboard loads, co-simulation of power conversion modules that form the electrical grid of an AES, and optimal control of a marine chiller that is directly applicable to other shipboard systems.

The DTMS framework came about because of the need to understand the dynamics of system-level thermal management. However, as system-level simulations in DTMS have become more complex, the need for more sophisticated control techniques has increasingly become apparent. Without a more sophisticated controls approach, it is the responsibility of the user to find suitable control coefficients for every controller in a simulation. When only one or two controllers are implemented, as in a standalone chiller simulation, this process is straightforward. However, simulations featuring many controllers, with many active loads, present real challenges. In addition, the adjustment of other user-defined parameters (design mass flow rates, initial conditions, etc.) affects control relationships as well. Before any attempt to simulate highly dynamic AES scenarios, it is recognized that a more robust control strategy must be developed and implemented. For example, allowing the user more freedom in controller type and open/closed loop setup would provide more flexibility in achieving stability and accuracy requirements. More sophisticated control analysis techniques, such as frequency response plotting and Model Predictive Control, could provide more effective tuning methods. In addition, advanced control approaches could streamline the interactions of several controllers into a single response. These approaches, and others, should be investigated in future work.

Finally, deliberations in the US Navy about whether an ac or dc power architecture is appropriate for the electrical distribution system aboard an AES are on-going. It is believed that these deliberations do not directly impact a physics-based approach to modeling of the electrical, thermal resistive, and thermal management frameworks in DTMS. Design of the thermal management network overlaying the electrical distribution system will be predicated on the thermal loads created by the electrical components. The number of components and their specific configuration, as well as bulk heat loads they present, will be the driving force behind the configuration of a thermal management system. When these important decisions have been made, it is our specific intent that this configuration is able to be simulated in a forthright manner.

Acknowledgements: This work was supported by the Office of Naval Research under auspices of the Electric Ship Research and Development Consortium (ESRDC). It represents the combined efforts of graduate research assistants Christopher Holsonback, Patrick Paullus, Patrick Hewlett, Matthew Pruske, Michael Pierce, and Gautam Salhotra over an extended period of time.

7 REFERENCES

[1] Pierce, R., "Thermal Management of the All-Electric Ship." MS Thesis, Naval Postgraduate School, 2004.

[2] van der Stelt, T., "TU-Delft Cycle-Tempo", http://www.3me.tudelft.nl/live/pagina.jsp?id=8c53f82e-a500-41f1-971b-629e832bfbef&lang=en, 2009.

[3] TRAX International, "Simulator Systems Portal", http://www.traxintl.com/simulator-systems, 2009.

[4] Paulus, P., "Creation of a Modeling and Simulation Environment for Thermal Management of an All-Electric Ship", Master's Thesis, University of Texas at Austin, December 2007.

[5] Pierce, M., and Kiehne, T. "DTMS: A framework for system-level, dynamic simulations across multi-disciplinary boundaries." Grand Challenges in Modeling and Simulation, Ottawa, Canada, July 2010.

[6] Salhotra, G., "Model-based Controller Design and Simulation of a Marine Chiller", Master's Thesis, University of Texas at Austin, August 2012.

[7] National Institute of Standards and Technology, "NIST Reference Fluid Thermodynamic and Transport Properties—REFPROP Version 8.0", Computer program, April 2007.

[8] Weisstein, E., "Newton-Cotes Formulas", MathWorld--A Wolfram Web Resource, 2009.

[9] Weisstein, E., "Backward Difference", MathWorld--A Wolfram Web Resource, 2009.

[10] Press, W., Teukolsky, S., Vetterling, W., Flannery, B., "Globally Convergent Methods for Nonlinear Systems of Equations", Numerical Recipes in C++: Art of Scientific Computing, 2nd ed. Cambridge Press, 2002.

[11] Holsonback, C. and Kiehne, T., "Thermal Aspects of a Shipboard Integrated Electric Power System." 6th IEEE Conference on Automation Science and Engineering, Toronto, August 2010.

[12] Hewlett, P. and Kiehne, T., "Dynamic Simulation of Ship-System Thermal Load Management", 6th IEEE Conference on Automation Science and Engineering, Toronto, August 2010.

[13] Pruske, M. and Kiehne, T., "Thermal-Electric Co-Simulation of Power Systems aboard an All-Electric Ship", Proceedings of Electric Machine Technology Symposium, Philadelphia, May 2010.

[14] Andrus, M., Woodruff, S., Steurer, M., Ren, W., "Crashback Simulations of a Notional Destroyer-Class All-Electric Ship", Advanced Naval Propulsion Symposium, 2006.

[15] Frank, M.V. and D. Helmick, "21st Century HVAC System for Future Naval Surface Combatants—Concept Development Report," NSWC Technical Report, September 2007.

[16] "RTDS Notional E-ship Model Technical Guide", Center for Advanced Power Systems, Florida State University, Tallahassee, Florida, Version 3.0, November 2006.

[17] Erickson, R. and Maksimovic, D., "Fundamentals of Power Electronics" 2nd Ed., Spring Science, 2001.

[18] Zivi, E., "Naval Combat Survivability Testbed MATLAB/Simulink Simulations", White Paper, May 2009.

[19] Serway, R., "Principles of Physics", 2nd Ed., London: Saunders College Pub., 1998.

[20] Ulaby, F., "Fundamentals of Applied Electromagnetics", Upper Saddle River, New Jersey, Prentice-Hall, 1999.

[21] Burton, L., "Multi-scale Thermal Modeling Methodology for High Power-Electronic Cabinets", Master's Thesis, Georgia Institute of Technology, December 2007.

[22] Zerby, M., King, K., Quinones, M., "Thermal Management Concepts for Configurable Zonal Systems Power Conversion Modules", CARDIVNSWC–TR-82-2000/25, Machinery Research and Development Directorate Technical Report, 2000.